공학박사 학위논문

Investigation on graphene growth for InGaN/GaN light emitting diodes

그래핀 성장과 이를 활용한 발광 다이오드의 제작

2015년 2월

서울대학교 대학원

나노융합학과

주 기 수

Investigation on graphene growth for InGaN/GaN light emitting diodes

그래핀 성장과 이를 활용한 발광 다이오드의 제작

지도교수 윤 의 준

이 논문을 공학박사학위 논문으로 제출함.

2015년 2월

서울대학교 대학원
나노융합학과

주 기 수

주기수의 박사학위 논문을 인준함
2015 년 2 월

위 원 장 박 원 철 인

부위원장 윤 의 준 인

위 원 송 윤 규 인

위 원 박 용 조 인

위 원 천 승 현 인

Abstract

Investigation on graphene growth for InGaN/GaN light emitting diodes

Kisu Joo
Department of Nano Science and Technology
Graduate School of Convergence Science and Technology
Seoul National University

Graphene is a two-dimensional carbon structure with great attraction for future-optoelectronics due to its excellent electrical, optical, and mechanical properties to apply for optoelectronics. Recently, many research groups have tried to apply graphene to optoelectronics. Especially transferred graphene released from Cu, Ni metal catalyst substrate is one of the most intensively studied materials in the context of optoelectronic devices. However, although graphene looks attractive to replace indium tin oxide (ITO) in optoelectronic devices, the luminous efficiency of light emitting diodes (LEDs) with graphene transparent conducting electrodes has been limited by degradation in graphene taking place during device fabrication.

In this study, I have tried to develop InGaN/GaN blue LEDs with single layer graphene released and transferred from Cu catalyst substrate. Chapter 1 and 2 introduce motivation of this study and describe various measurement, respectively. In chapter 3, I will report the high quality single layer graphene grown method by plasma enhanced chemical vapor deposition (PECVD) and analyze its resulting graphene with Raman spectroscopy, AFM, TEM, and hall measurement.

In chapter 4, I will report the problem of previous fabrication method for LEDs with graphene films as transparent conductive electrode, and demonstrate the high performance InGaN/GaN blue LEDs with single layer graphene by avoiding graphene damages during LED fabrication process. Properties of graphene after the device fabrication were a critical factor affecting the performance of GaN-based LEDs. It was found that during the fabrication graphene was severely damaged and split into submicrometer-scale islands bounded by less conducting boundaries when graphene was transferred onto LED structures prior to the GaN etching process for p-contact formation. On the other hand, when graphene was transferred after the GaN etch and p-contact metallization, graphene remained intact and the resulting InGaN/GaN LEDs showed electrical and optical properties that were very close to those of

LEDs with 200 nm thick ITO films. The forward-voltages and light output powers of LEDs were 3.03 V and 9.36 mW at an injection current of 20 mA, respectively.

In chapter 5, directly grown graphene growth method and its resulting LEDs will be introduced in detail. I will demonstrate graphene growth method to directly define it without metal catalyst such as Cu or Ni substrate and additional transfer process to remove the Cu or Ni metal substrate. Direct graphene growth without a catalyst is possible on a variety of substrates including transparent and flexible ones at temperatures as low as 500 ℃ using plasma enhanced chemical vapor deposition. The film consists mainly of few-layer polycrystalline graphene, confirmed by transmission electron microscopy and Raman spectra. With the few-layer graphene directly grown on GaN substrates, light emitting diodes could be fabricated without transfer process and resulted in uniform output power over tens of devices. These show that direct graphene growth provides advantage of uniform interface and reliable performance in addition to transferfree device fabrication, which can be adopted easily in the industrialization of graphene

---

Kew words:

Light emitting diodes (LEDs), direct graphene growth, reduced graphene damage.

Student ID: 2009-31186

Contents

List of Figures

List of Table

Chapter 1

Introduction

1.1. Background of graphene

Graphene is the name given to a monolayer of carbon atoms tightly bonding of sp^2, which packed into a two-dimensional honeycomb lattice. It is a basic building block for other graphitic materials. Before 2004, the isolation of stable sheets of graphene was not thought possible. However, Andre Geim and Konstantin Novoselov from the University of Manchester (UK) succeeded to obtain a single layer graphene []. They used mechanical exfoliation method for extracting thin layers of graphene from a graphitic crystal with Scotch tape, and then transfer these to a silicon wafer. Figure 1 (adapted from reference 1) shows some graphene from single to thick layers which transferred by mechanical exfoliation technique [1]. It can be compared highly transparent, crystalline shapes and little color with the rest of the wafer. The step-like pattern is a pile of graphene sheets layered on top of one another.

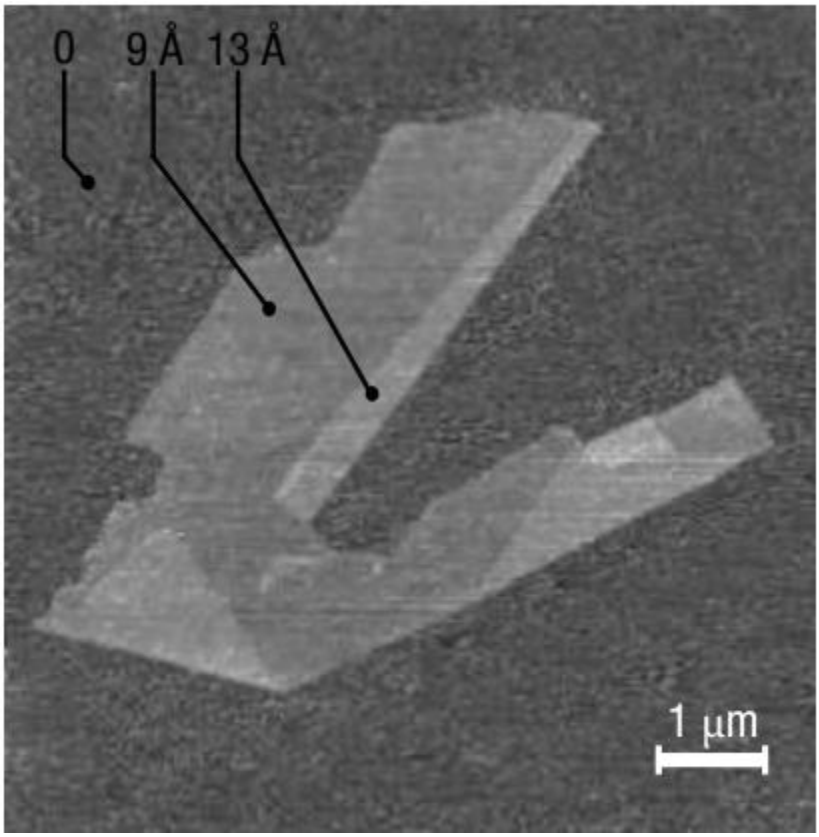

Figure 1. 1. One-atom-thick single crystals: Graphene visualized by atomic force microscopy

Graphene has several different properties compare with other materials. It is extremely thin (one atomic layer), mechanically very strong, transparent and flexible conductor. Especially, a superiority of the electronic properties and transparency of graphene attracts enormous interest. So far, the main focus has been mainly on fundamental physics and electronic devices. Its true potential lies in optoelectronics and photonics, where the combination of its unique optical and electronic properties can be fully exploited such as flexible touch screens, organic light emitting diodes, solid-state LEDs and so on.

Mechanical properties
Tensile strength: 130 GPa [2]
Young's modulus: 1 TPa [3]
Tension rigidity: 340 GPa·nm [2]
Thermal conductivity: 2-4 $kW \cdot m^{-1}K^{-1}$ (freely suspended graphene) [4]
Distance between adjacent layers of graphene in graphite: 3.4 Å [5]
Electrical properties
Band gap: 0 eV (in sheet graphene) [6]
Band gap: ~3.8 eV (in graphene ribbons) [6]
Electron mobility: ~200,000 $cm^2 \cdot V^{-1} \cdot s^{-1}$ (intrinsic limit) [1]
Electron mobility: ~40,000 $cm^2 \cdot V^{-1} \cdot s^{-1}$ (on SiO_2 substrate) [1]
Carrier density: 10^{12} cm^{-2} [7]
Free path for electron-acoustic phonon scattering: >2 μm [7]
Optical properties
White light absorption: 2.3 % [8]
White light transmission: 97.7 % [9]

Table 1. General properties of graphene

1.2. Current progress on LEDs with graphene

Optoelectronic devices such as light-emitting diodes (LEDs) have received vast attention to the research and development sector. Indium tin oxide (ITO) is conventionally used as the transparent conducting electrode for these devices, but ITO is expensive, and shows relatively poor transparency in the ultra violet, visible and near-infrared light ranges, and instability in the presence of acids or bases. Therefore, there exist significant needs for a novel electrode material that can replace ITO for application in optoelectronic devices.

To date, Jo *et al.*, reported that transparent graphene films have been successfully transferred onto various foreign substrates [10]. They demonstrate a large-scale batch fabrication of GaN LEDs with patterned multi-layer graphene (MLG) as transparent conducting electrodes. MLG films were synthesized using a CVD technique on nickel films and transferred onto target LED substrate by utilizing conventional PMMA assisted transfer method. Moreover, MLG films showed a sheet resistance of ~ 620 Ω/sq with a transparency of more than 85% in the 400~800 nm wavelength range. They have tried to apply graphene electrodes to solid-state LEDs as a transparent

conducting electrode of GaN-based blue LEDs. However, due to the higher sheet resistance and not clear interface between graphene films and p-GaN surface, the light output power performance was relatively poor than that of LEDs with ITO electrode and showed non-uniformed light emitting patterns by resulting LEDs with MLG.

Seo *et al.,* demonstrated a current spreading electrode combining ITO nanodots and graphene [11]. They reported a device that combines ITO nanodot nodes with two-dimensional chemically converted graphene (CCG) films to yield a GaN-based to apply for the potential use in the ultraviolet region. ITO nanodot nodes were employed to enhance the sheet resistance of transparent metal layers and provide clean interface between CCG and p-GaN layer. Despite higher sheet resistance and transparency of CCG films of 2.2×10^3 Ω/sq and 85% transmittance at 550 nm, resulting L-I-V characteristics of UVLEDs with mixture of CCG films and ITO nanodot showed very close ones could be compared to those of LEDs with planar ITO films.

Also, Lee *et al.,* reported that reduced contact resistance by inserting Ni/Au films between graphene and a p-type GaN layer and obtained enhanced electroluminescent intensity [12]. Their group designed new scheme of transparent conducting layer by incorporating thin metal layer into interface

between graphene and p-GaN layer. As a result, contact resistance measured by transmission line method (TLM) reduced from 5.5 to 0.6 Ω/cm^2 without critical optical loss. Resulting LEDs with metal-graphene mixed layer provided current spreading and injection into the p-type GaN layer, enabling three times enhanced electroluminescent intensity compared with those with graphene electrodes alone.

1.3. Reference

[1] A. K. Geim and K. S. Novoselov, *Nat Mater* **6**, 183-191 (**2007**).

[2] G. Tsoukleri, J. Parthenios, K. Papagelis, R. Jalil, A. C. Ferrari, A. K. Geim, K. S. Novoselov and C. Galiotis, *Small* **5**, 2397-2402 (**2009**).

[3] C. Lee, X. D. Wei, J. W. Kysar and J. Hone, *Science* **321**, 385-388 (**2008**).

[4] E. Pop, V. Varshney and A. K. Roy, *Mrs Bull* **37**, 1273-1281 (**2012**).

[5] A. H. Castro Neto, F. Guinea, N. M. R. Peres, K. S. Novoselov and A. K. Geim, *Rev Mod Phys* **81**, 109-162 (**2009**).

[6] M. S. Fuhrer, *Science* **340**, 1413-1414 (**2013**).

[7] A. Akturk and N. Goldsman, *J Appl Phys* **103**, 053702 (**2008**).

[8] R. R. Nair, P. Blake, A. N. Grigorenko, K. S. Novoselov, T. J. Booth, T. Stauber, N. M. R. Peres and A. K. Geim, *Science* **320**, 1308-1308 (**2008**).

[9] P. Blake, E. W. Hill, A. H. Castro Neto, K. S. Novoselov, D. Jiang, R. Yang, T. J. Booth and A. K. Geim, *Appl Phys Lett* **91**, 063124 (**2007**).

[10] G. Jo, M. Choe, C. Y. Cho, J. H. Kim, W. Park, S. Lee, W. K. Hong, T. W. Kim, S. J. Park, B. H. Hong, Y. H. Kahng and T. Lee, *Nanotechnology* **21**, 175201 (**2010**).

[11] T. H. Seo, K. J. Lee, T. S. Oh, Y. S. Lee, H. Jeong, A. H. Park, H. Kim, Y. R. Choi, E. K. Suh, T. V. Cuong, V. H. Pham, J. S. Chung and E. J. Kim, *Appl Phys Lett* **98**, 251114 (**2011**).

[12] J. M. Lee, H. Y. Jeong, K. J. Choi and W. Il Park, *Appl Phys Lett* **99**, 041115 (**2011**).

Chapter 2

Growth tool and analysis method

2.1. Growth tools

2.1.1. PECVD system

Plasma-assisted thermal chemical vapor deposition, also known as plasma enhanced chemical vapor deposition (PECVD) or Inductively coupled plasma chemical vapor deposition (ICPCVD), is an one kind of chemical vapor deposition method used to form single or few layers graphene films recently. It is well known that graphene growth can be made in relatively low temperature thanks to the plasma-assisted process. Moreover, plasma enhanced chemical vapor deposition has been intensively developed to grow graphene on a large scale [1]. This method can be executed at a lower temperature than that required for previous growth. Nickel and copper catalyst substrates are commonly used metal those for growth of graphene [2, 3]. Due to the different growth mechanisms in copper and nickel catalytic

syntheses [4], the number of graphene films grown on the hosts is quite different from each other. In this study, Cu foil was adopted to grow single layer graphene to utilize graphene as an transparent conductive electrodes.

Figure 2.1 shows image of ICPCVD system. RF coil is mounted at the top of the chamber. Figure 2.2a shows schematic diagram of the inductively coupled plasma chemical vapor deposition (ICP-CVD) system. RF coil is mounted at the top of the chamber. Inlet ports were installed at the top of the chamber to allow gases to flow into the chamber. The gas flow is controlled by a mass flow controller (MFC). Plasma is generated by applying 13.56 MHz RF bias power to the RF coil.

To investigate the heating effect of substrate by RF plasma, the substrate temperature is monitored under different plasma powers of 50 and 400 W. It is conducted without filament heating of substrate and the temperature is measured by a K-type thermocouple which is attached to substrate. When the plasma power is 400 W, the temperature increases only about 3 ℃ after 12 minutes (Figure 2.1b). When the plasma power is reduced to 50 W, the temperature does not change after 14 minutes. Considering the plasma powers (~50 W) used in the graphene growth, we conclude that the substrate heating effect by RF plasma is negligible in our system.

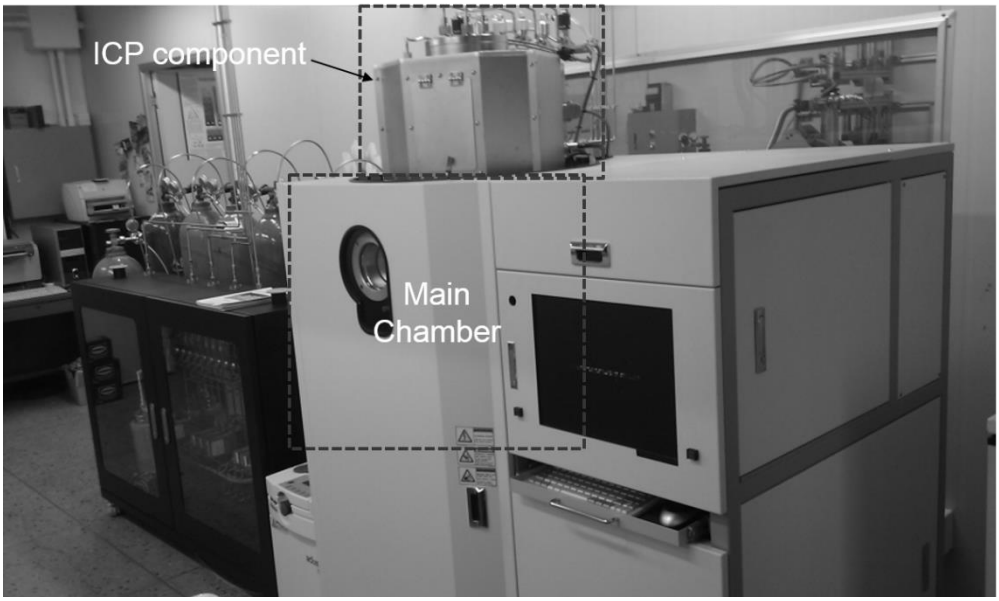

Figure 2. 1. PECVD (ICP-CVD) system

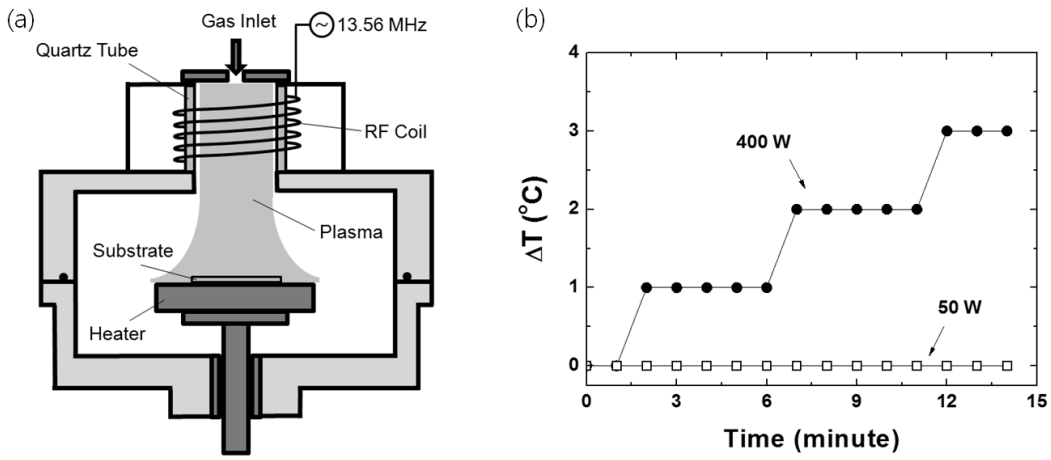

Figure 2. 2. (a) Schematic diagram of ICP-CVD system. (b) Substrate heating effect by plasma under different plasma power of 50 and 400 W.

2.1.2. MOCVD system

Metalorganic vapour phase epitaxy (MOVPE), also known as organometallic vapour phase epitaxy (OMVPE) or metalorganic chemical vapour deposition (MOCVD), is a chemical vapor deposition method used to produce single or polycrystalline thin films. It is a highly complex process for growing crystalline layers to create complex semiconductor multilayer structures. In contrast to molecular beam epitaxy (MBE) the growth of crystals is by chemical reaction and not physical deposition. This takes place not in a vacuum, but from the gas phase at moderate pressures (10 to 760 Torr). As such, this technique is preferred for the formation of devices incorporating thermodynamically metastable alloys, and it has become a major process in the manufacture of optoelectronics.

In this study, Thomas Swan 3 x 2'' (incorporated 3 substrates of 2 inch size) close coupled showerhead (CCS) MOCVD system was used to grow GaN based nitride epitaxial layer to perform transmission line method (TLM). Trimethylgallium(TMGa,$(CH_3)_3Ga$)) and Trimethylindium(TMIn, $(CH_3)_3In$) were used for group III sources. Solkatronics Blue-Ammonia(NH_3) of

99.9999% purity was used for group V sources.

Bis(cyclopentadienyl)magnesium (Cp_2Mg, $(C_2H_5)_2Mg$) and 10 ppm diluted silane(SiH_4) was installed for p-type and n-type doping, respectively. Schematic of gas delivery system of MOCVD is in Figure 2.3. The reactor pressure is kept at 50 mbar which is controlled by vacuum pump and throttle valve. Substrates are loaded on a susceptor equipped with a special rotating system for uniform temperature during the growth. The susceptor consists of a rotating planetary disk (main rotation) which is driven by an electric motor and satellite disks. The satellite disks which hold the substrates are arranged concentrically on the planetary disk. It is designed for loading 3 substrates of 2 inch simultaneously. An RF inductor is used to heat the reactor. It is mounted on a height adjustable ceramic holder, below the susceptor in the reactor housing.

Figure 2. 3. MOCVD system

2.2. Method

2.2.1. Fabrication of light emitting diode

Included here is some general information about the equipments for the LED fabrication process.

1) Track system: for coating, developing and removing of PR and soft and hard baking process

2) Mask aligner: UV exposure with designed masks for metal electrodes and passivation layer forming for mesa etch

3) E-beam evaporator: for single or multi-layer complex metal structure for transparent conductive metal or ohmic contact structure

4) Rapid thermal annealing (RTA): for annealing the sample

1× 1 mm^2 LEDs chip were fabricated by using photolithography, dry etch, and metallization process. All of the fabrication processes were performed at

the Korea Advanced Nano Fab Center (KANC) with conventional process for LEDs.

At first, in order to expose n-type GaN layer to the top, passivation masks for the mesa etch region were performed by track system and mask aligner. AZ7550 (AZ electronic Materials) was used to define mesa structure with the height of 3 μm. Finishing the PR forming for mesa etch, the height and mesa slope angle were measured by surface profiler and optical microscope.

ICP etch was made to expose an n-type GaN layer by using ICP etch system (STS, Multiplex ICP system) at a bias power of 100 W and ICP power of 800 W. A mixed gas (Cl_2 : BCl_3 = 30 sccm : 5 sccm) was introduced during the etch process. A 500 nm thick GaN layer was etched for 100 sec. Measured etch rate of GaN layer is 4.16 nm / sec. To remove the residual PR O_2 ashing process was fulfilled by PVA Tepla 300 Microwave Plasma System.

Subsequently, the electron beam evaporation method (ULTECH, SEE-7D series) was used to deposit a Ti/Al/Ti/Au (30/100/30/100 nm) complex metal structure for ohmic contact to n-type GaN, and a Ti/Au (30/100 nm) bi-metal layer for current spreading electrodes.

2.2.2. Raman spectroscopy

In order to understand of Raman signal from the graphene sample, an understanding of the phonon dispersion of graphene is essential to interpret the Raman spectra of graphene. Many researcher has studied about the Raman spectra of the graphene. Here, I will write the brief contents of the G, D and 2D band of graphene cited from the paper titled "Raman spectroscopy in graphene", Physics Reports, 473, 51-87 (2009). To further information about Raman spectra of the graphene in detail, refer to the article written by L.M.Malard *et al*,.

In reciprocal space, the unit cell is as shown in Figure 2.4(e) for monolayer and bilayer (1-LG and 2-LG), and is planar, though atomic motion in the z direction normal to the plane would require a third direction. Figure 2.4(e) also shows some high symmetry points within the first Brillouin zone of monolayer graphene: The Γ point at the zone center, the M points in the middle of the hexagonal sides and the K and K' points at the corners of the hexagons. Notice that K and K' are inequivalent since they are not connected by the unit vectors of the reciprocal lattice. In contrast, 3-LG and 4-LG

reciprocal space requires a plane for $k_z = 0$ and $k_z = \pi/c$ forming the lower and upper planes of the Brillouin zone (BZ) for 3D graphite, as shown in Figure 2.4(f). In turbostratic graphite, denoted by 2D graphite, there is no stacking order between adjacent graphene layers and the interlayer spacing (>0.342 nm) is larger than that for crystalline graphite (c/2 = 0.335 nm). The absence of stacking order between the graphene planes results in 2D graphite having modified physical properties relative to 3D crystalline graphite. Crystalline 3D graphite is found in nature as a natural mineral, or is prepared from precipitants coming from steel-making, and these flakes are called ``kish'' graphite. Another common form of crystalline graphite is highly oriented pyrolytic graphite (HOPG), which is a synthetic AB stacked graphite obtained from carbon-based precursors, and heat treated at various high temperatures (over 3200 ^{o}C under pressure).

An understanding of the phonon dispersion of graphene is essential to interpret the Raman spectra of graphene. Since the unit cell of monolayer graphene contains two carbon atoms, A and B, there are six phonon dispersion bands (see Figure 2.5), in which three are acoustic branches (A) and the other three are optic (O) phonon branches. For one acoustic branch (A) and one optic (O) phonon branch, the atomic vibrations are perpendicular to the

graphene plane, and they correspond to the out-of plane (o) phonon modes. For two acoustic and two optic phonon branches, the vibrations are in-plane (i). Traditionally, the directions of the vibrations are considered with respect to the direction of the nearest carbon-carbon atoms and, therefore, the phonon modes are classified as longitudinal (L) or transverse (T) according to vibrations parallel with or perpendicular to, respectively, the A-B carbon-carbon directions. Therefore, along the high symmetry ΓM and ΓK directions, the six phonon dispersion curves are assigned to LO, iTO, oTO, LA, iTA, and oTA phonon modes. (see Figure. 2.5)

To correctly describe the dispersion of the LO and iTO phonon branches near the k_z and K points, it is important to consider the renormalization of the phonon energies, associated with a process in which a phonon can create an electron-hole pair (similarly to the creation of an electron-positron pair by a photon in quantum electrodynamics) [5]. This important electron-phonon coupling cannot be understood within the framework of the Born-Oppenheimer approximations, and gives rise to an interesting effect known as the Kohn anomaly [6]. The Kohn anomaly is responsible for a softening of certain Γ and K point phonons [7].

The most prominent features in the Raman spectra of monolayer graphene are the so-called G band appearing at 1582 cm^{-1} (graphite) and the G' band at about 2700 cm^{-1} using laser excitation at 2.41 eV (see for example, Figure 2.6). In the case of a disordered sample or at the edge of a graphene sample, we can also see the so-called disorder-induced D-band, at about half of the frequency of the G' band (around 1350 cm^{-1} using laser excitation at 2.41 eV).

The G band is associated with the doubly degenerate (iTO and LO) phonon mode (E_{2g} symmetry) at the Brillouin zone center. In fact, the G-band is the only band coming from a normal first order Raman scattering process in graphene. On the other hand, the G' and D-bands originate from a second-order process, involving two iTO phonons near the K point for the G' band or one iTO phonon and one defect in the case of the D-band. Since the G' band is approximately twice the D band frequency, some authors prefer to call it the 2D band. However, this two-phonon band is allowed in the second order Raman spectra of graphenes without any kind of disorder or defects. In order to prevent any misleading connection of this feature with disorder or defects, and to avoid confusion between the designation of "2D" to denote two dimensionality, we will use here the conventional notation "G'-band" as is used in the graphite and nanotube literature.

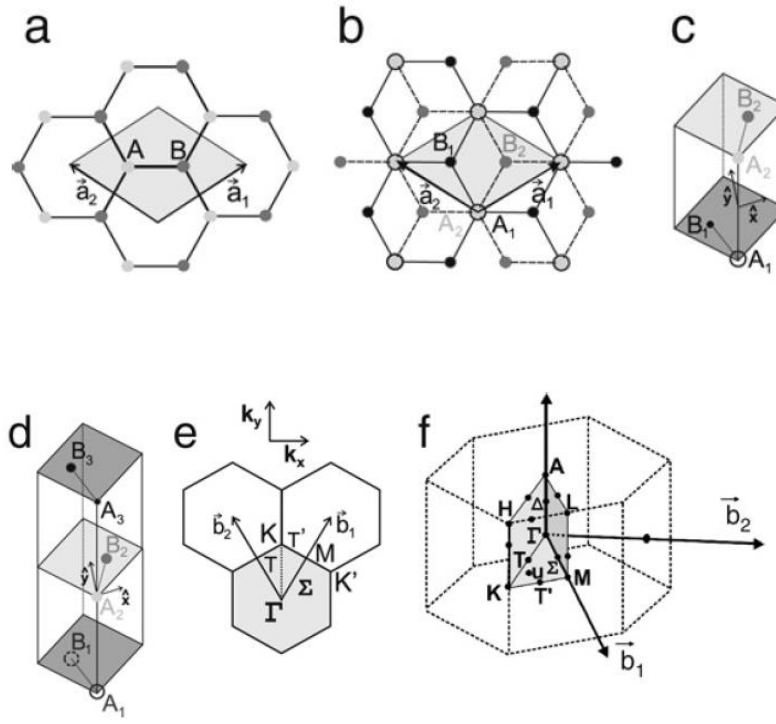

Figure 2. 4. (a) A top view of the real space unit cell of monolayer graphene showing the inequivalent atoms A and B and unit vectors a_1 and a_2. (b) A top view of the real space of bilayer graphene. The light/dark gray dots and the black circles/black dots represent the carbon atoms in the upper and lower layers, respectively, of bilayer graphene (2-LG). (c) The unit cell and the x and y unit vectors of bilayer graphene and (d) the same as (c) but for trilayer graphene. (e) The reciprocal space unit cell showing the 1st Brillouin zone with its high symmetry points and lines, such as T connecting **Γ** to K; Σ connecting

Γ to M; T' connecting K to M. The two primitive vectors b_1 and b_2 are shown and the two vectors on the top of the three hexagons show the reciprocal space coordinate axes. (f) The Brillouin zone for 3D graphite, showing the high symmetry points and axes. Here Δ is a high symmetry point along the axis connecting points A and **Γ**, and u is a point in the KM**Γ** plane.

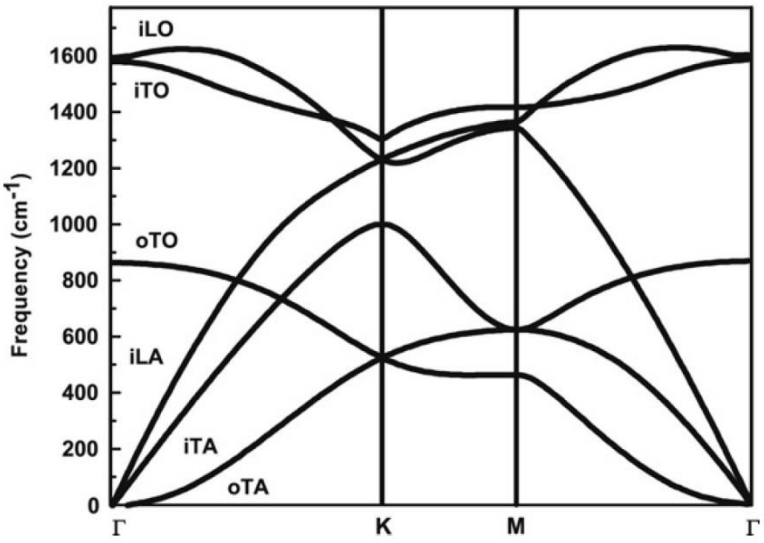

Figure 2. 5. Calculated phonon dispersion relation of graphene showing the iLO, iTO, oTO, iLA, iTA and oTA phonon branches

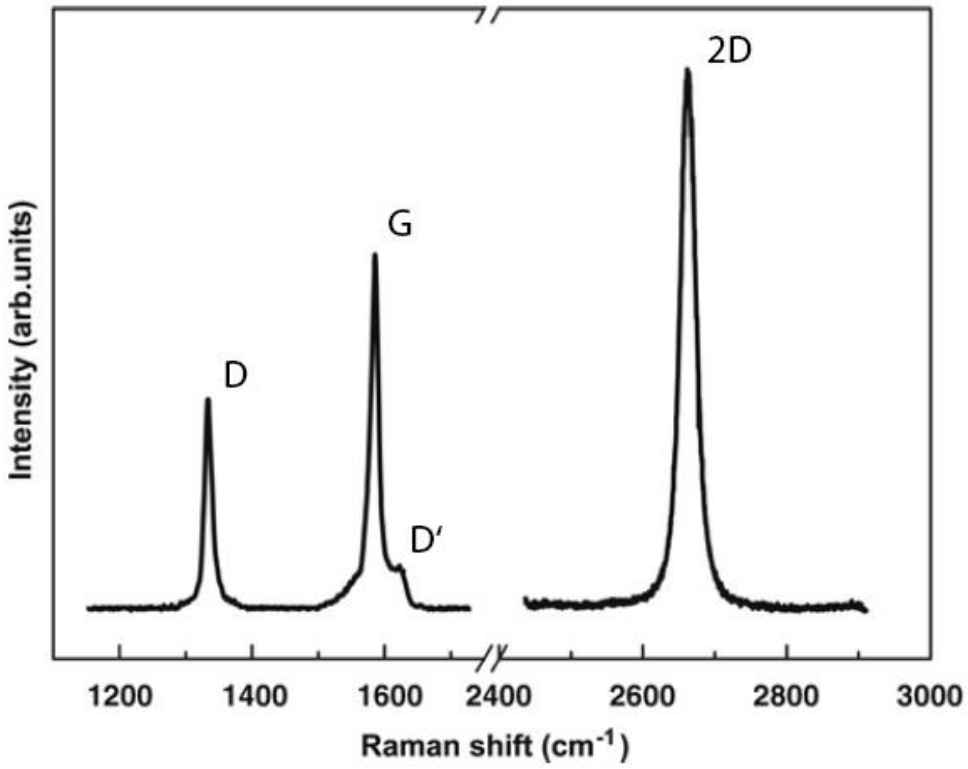

Figure 2. 6. Raman spectrum of a graphene edge, showing the main Raman features, the D, G and G0 bands taken with a laser excitation energy of 2.41 eV.

2.2.3. Hall Effect

In a magnetic field, a moving charge experiences a Lorentz force. Using the Drude model with an applied magnetic field (*B*), the current density is defined as:

$$\vec{J} = \frac{1}{\rho_0}\left(\vec{E} - \frac{1}{ne}\vec{j}\times\vec{B}\right) \qquad \text{(eq. 1.1)}$$

which can be rewritten as:

$$\vec{E} = \rho_0\vec{j} + \frac{1}{ne}\vec{j}\times\vec{B} \qquad \text{(eq. 1.2)}$$

We can then formulate this equation in matrix form using Cartesian coordinates and under the assumption that we have a 2D system with a B field in the z direction and current in the xy plane. Doing so we get:

$$\begin{pmatrix} E_x \\ E_y \end{pmatrix} = \begin{pmatrix} \rho_0 & \frac{B}{ne} \\ -\frac{B}{ne} & \rho_0 \end{pmatrix} \begin{pmatrix} j_x \\ j_y \end{pmatrix} \qquad \text{(eq. 1.3)}$$

Referring to Figure 2.4, we can define the Hall resistance, R_H, as:

$$R_H \equiv \frac{V_h}{I} \qquad \text{(eq. 1.4)}$$

where:

$$V_h = \int E_y \cdot dl \qquad \text{(eq. 1.5)}$$

With no current flow in the y direction (1.7) simplifies to:

$$E_y = -\frac{B}{ne} j_x \qquad \text{(eq. 1.6)}$$

Plugging (1.6) into (1.5) we can get:

$$V_h = \int \frac{B}{ne} j_x dl = \frac{B}{ne} j_x W \qquad \text{(eq. 1.7)}$$

In two dimensions the current density is defined as:

$$j_h \equiv \frac{I}{W} \qquad \text{(eq. 1.8)}$$

Using this fact along with the definition for the Hall voltage in (1.4) we have that:

$$R_H \equiv \frac{B}{ne} \qquad \text{(eq. 1.9)}$$

By sweeping a perpendicular magnetic field, *B*, and measuring R_H one can determine the carrier density (*n*). You can then use this density and the measured longitudinal resistivity (ρ) to measure the sample's mobility (μ).

Moreover, transverse voltage is the Hall voltage (V_H) and its magnitude is equal to

$$\frac{IB}{ned} \qquad \text{(eq. 1.10)}$$

where d is the sample thickness.

In some cases, it is convenient to use layer or sheet density (n_s) instead of bulk density.

$$n_s = nd \qquad \text{(eq. 1.11)}$$

Then, we can obtain the equation

$$n_s = \frac{IB}{e|V_H|} \qquad \text{(eq. 1.12)}$$

Therefore, by measuring the Hall voltage V_H and from the known values of I, B, and e, we can determine the sheet density (n_s) of charge carriers. The sheet resistance (R_S) of the graphene can be determined by use of this hall measurement technique.

$$\mu = \frac{|V_H|}{R_S IB} = \frac{1}{en_S R_S} \qquad \text{(eq. 1.13)}$$

If the conducting layer thickness d is known, one can determine resistivity (r).

$$r = R_S d \qquad \text{(eq. 1.14)}$$

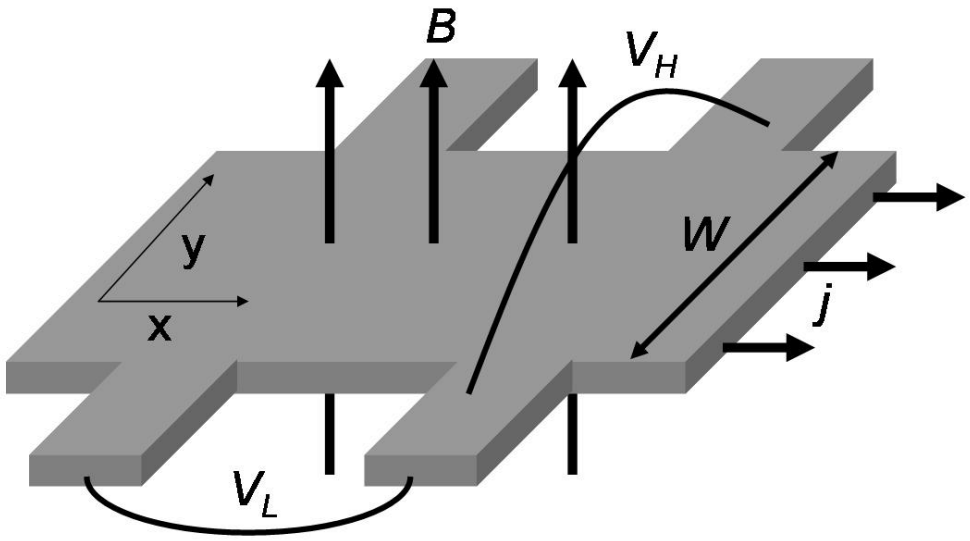

Figure 2. 7. Hall Bar geometry

2.2.4. Transmission line method

The ohmic contacts are of great importance in relation with the quality and the reliability of the microelectronic devices. The resistance of an ohmic contact can be evaluated by the transmission line method (TLM). The TLM structure is a series of identical contact pads, of width (w) and length (L_C), spaced at varying intervals d_1, d_2, d_3, d_4… as shown in Figure 2.5.

As shown in Figure 2.5a, Sample is fabricated and measured at each distance in terms of R with 2 point probe method. Then, by using Figure 2.5b we can obtain L_T, R_C and R_S, respectively. The TLM analysis yields the following relations:

$$R(L) = \frac{R_S}{W}\left(L + 2L_T\right) \qquad \text{(eq. 1.15)}$$

$$R(L=0) = 2R_C = \frac{R_S}{W} \times 2L_T \qquad \text{(eq. 1.16)}$$

Solving equation for R_S yields:

$$R_S = \frac{R_C W}{L_T} \qquad \text{(eq. 1.17)}$$

Specific contact resistance:

$$\rho_C = R_S \times L_T{}^2 \qquad \text{(eq. 1.15)}$$

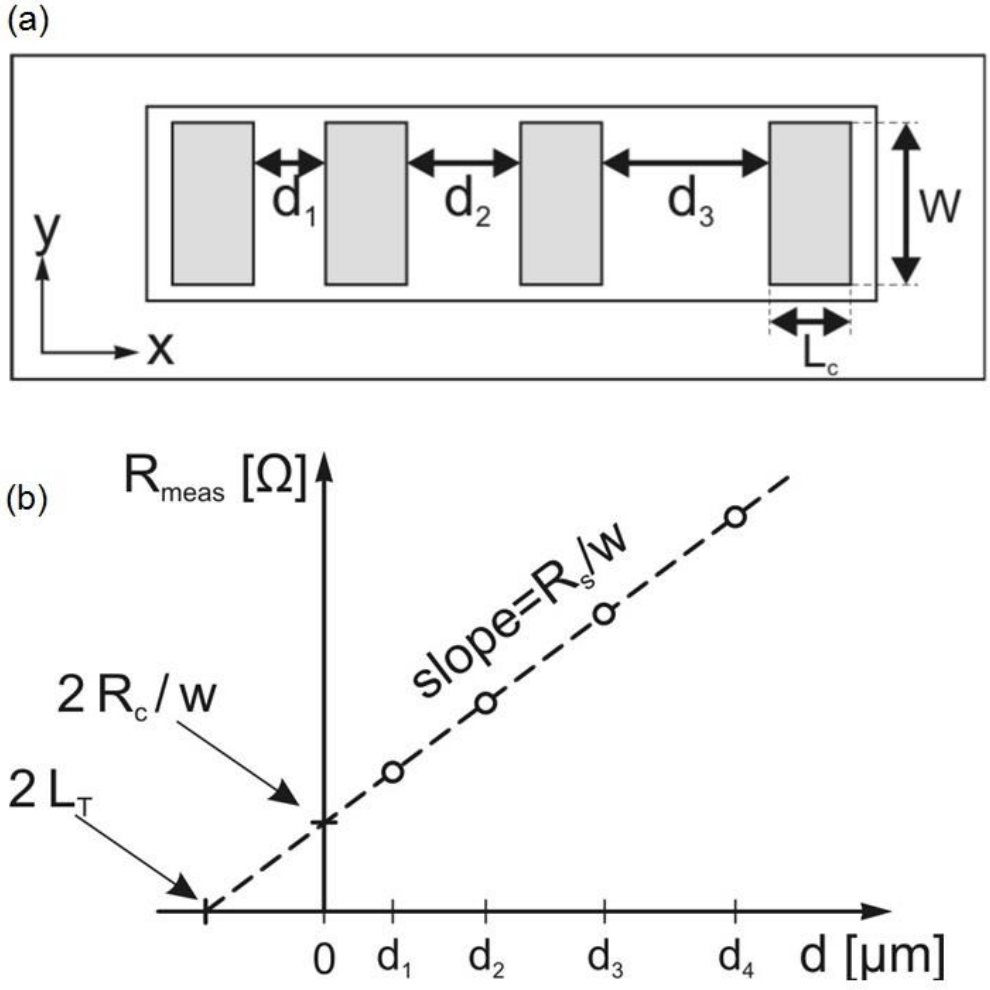

Figure 2. 8. (a) TLM pattern: contact resistance test patterns (b) Evaluation of the contact and sheet resistances for TLM measurements

2.3. Measurement tools

2.3.1. Field emission scanning electron microscopy (FE-SEM)

The size and shape of nanospheres in this study are measured by FESEM. The clear images of nanospheres including polystyrene/silica nanospheres, and polystyrene/silica/alumina nanospheres, are obtained with a Hitachi S-4300SE.
.

2.3.2. Transmission electron microscopy (TEM)

The TEM specimens were prepared by using focused ion beam (FIB). The images of cross-sectional transmission electron microscopy (XTEM) were observed by a JEOL JEM-2100F in Korea Advanced Nano Fab Center. Bright and dark field techniques were used to observe the vertical structure of graphene and GaN epitaxial layer. Selective area diffraction patterns (SADPs) from graphene layers were obtained from TEM with an appropriate aperture.

2.3.3. Photoluminescence (PL)

PL spectroscopy is a contactless, nondestructive method of probing the electronic structure of materials. Specifically, light is directly onto a sample, where it is absorbed and imparts excess energy into the material in a process

called “photo-excitation”. One way this excess energy can be dissipated by the sample is through the emission of light or luminescence. In the case of photo-excitation, this luminescence is called photoluminescence (PL). The intensity and spectral content of this PL is a direct measure of various important material properties. PL measurements were made at room temperature using 325 nm line of He-Cd laser was used. The PL signal was dispersed by a SPEX monochromator and detected by liquid-nitrogen-cooled charge coupled device (CCD) detector.

2.3.4. High resolution X-ray diffraction (HR-XRD)

Panalytical X’pert instrument was used for HR-XRD measurement and ω-scan. The angle divergence of 12 arcsec or less can be obtained by 4 bounce Ge 022 channel cut monochromator.

2.3.5. Atomic force microscopy (AFM)

AFM measurements were performed in an atmospheric ambient to investigate surface morphology of graphene and c-plane GaN sample. The Au-coated Si probes were used in noncontact mode using PSI-XE100 system. For statistical analyses, Nanotec WSxM v4.0 was used.

2.3.6. UV-visible spectrophotometer

To evaluate the optical characteristics of graphene films, reflectance and transmittance were measured by using an integrating sphere by collecting photons scattered from all the angles. The measured wavelength of GaN was range from 300 nm to 900 nm.

2.3.7. Raman spectroscopy

inVia Raman microscopes from RENISHAW were utilized to evaluate the changes of characteristics of graphene before and after transfer procedure or growth, Light source was used with an excitation wavelength of 514.5 nm. The size of laser spot measured on sample stage is around ~ 1× 1 μm^2.

2.3.8. L-I-V measurement

The *L-I-V* characteristics and electroluminescence spectra were obtained by a Keithley 2425 source measurement unit and a Newport 1936-C spectroradiometer.

2.3.9. Residual gas analyzer (RGA)

A residual gas analyzer (RGA 100, Stanford Research Systems) is attached at the main chamber to investigate the mass spectra of discharged species. The high pressure of ~10^{-2} Torr during the graphene growth is not suitable for the measurement because the RGA system requires a high vacuum (<10^{-4} Torr) environment.

2.4. Reference

[1] Y. S. Kim, J. H. Lee, Y. D. Kim, S. K. Jerng, K. Joo, E. Kim, J. Jung, E. Yoon, Y. D. Park, S. Seo and S. H. Chun, *Nanoscale* **5**, 1221-1226 (**2013**).

[2] M. P. Levendorf, C. S. Ruiz-Vargas, S. Garg and J. Park, *Nano Lett* **9**, 4479-4483 (**2009**).

[3] G. Jo, M. Choe, C. Y. Cho, J. H. Kim, W. Park, S. Lee, W. K. Hong, T. W. Kim, S. J. Park, B. H. Hong, Y. H. Kahng and T. Lee, *Nanotechnology* **21**, 175201 (**2010**).

[4] X. S. Li, W. W. Cai, L. Colombo and R. S. Ruoff, *Nano Lett* **9**, 4268-4272 (**2009**).

[5] G. G. Samsonidze, E. B. Barros, R. Saito, J. Jiang, G. Dresselhaus and M. S. Dresselhaus, *Phys Rev B* **75**, (**2007**).

[6] W. Kohn, *Phys Rev Lett* **2**, 393-394 (**1959**).

[7] S. Piscanec, M. Lazzeri, F. Mauri, A. C. Ferrari and J. Robertson, *Phys Rev Lett* **93**, (**2004**).

Chapter 3

Single layer graphene growth

3.1. Introduction

Graphene is anticipated to play a key role in foreseeable future usage as a valuable component in electronics and optoelectronics due to its excellent electrical, optical, and mechanical properties [1-6]. Graphene has been prepared by several techniques, including (i) precipitation on a silicon carbide surface [7], (ii) mechanical exfoliation from graphite [1], (i ii) reduction of exfoliated graphene oxide [8], and (iv) growth by chemical vapor deposition (CVD) on catalytic metal surfaces [9-12]. Among these, graphene films grown by CVD on catalytic metal surfaces is especially interesting for the purpose of constructing electrodes, because it has been successfully used to grow large-scale, conductive, and transparent graphene films from catalytic reactions that can be transferred onto arbitrary substrates [9]. Optoelectronic devices such as light-emitting diodes (LEDs) have received vast attention from the research and development sector [13] [14]. Indium tin oxide (ITO) is

widely used as the transparent conducting electrode for these devices, but ITO is costly, and shows poor transparency in the blue and near-infrared light ranges, instability in the presence of acids or bases, and susceptibility to ion diffusion into the substrate [15, 16]. Therefore, there is a significant need for a novel electrode material that can replace ITO for application in optoelectronic devices. To this end, graphene based transparent electrodes have attracted significant attention for their advantages in material properties mentioned above. Several pioneering works have reported the application of graphene-based thin films as transparent electrodes of organic solar cells, liquid crystal displays, and organic LEDs [16, 17].

In chapter 3, it will be introduced that single layer graphene has been synthesized on Cu foil with PECVD system to apply for InGaN/GaN LEDs to achieve the superior properties comparable to those of ITO-LEDs.

3.2. Experimental procedure

25 μm-thick Cu foils (Alfa Aesar, 99.8%, #13382) were prepared as the metal catalyst substrates. The entire growth process for the single layer graphene was performed using a PECVD (A-tech system,) with argon, hydrogen, oxygen, and methane gas.

The chamber is pumped with a turbomolecular pump (Osaka Vacuum LTD, TG1003), keeping the base pressure as low as ~ 10^{-7} Torr. Polycrystalline Cu foil was cut into 7 × 7 cm^2 pieces and mounted in the chamber without any pre-cleaning treatment. Five different stages were employed to grow graphene films on Cu foil suing methane (CH_4) as a carbon source. The Cu substrate was heated to the growth temperature (700 ~ 830 ℃) at a heating rate of 3 ℃ s^{-1}. When it reached the target temperature, H_2 gas was introduced into the chamber at a flow rate of 40 standard cubic centimeters per minute (sccm). Hydrogen gas was discharged by an RF power of 50 W for 2 minutes to eliminate surface oxides on the copper foil. Then, the chamber was purged with Ar at a flow rate of 100 sccm for 2 minutes to remove residual hydrogen gas. During the graphene growth stage, radio-frequency (RF) plasma was generated for a specified growth time under a continuous flow of argon (or

hydrogen, 40 sccm) and methane (1 sccm), while the pressure was kept at 10 mTorr. The plasma power was varied from 10 to 200 W and the growth time was varied from 0.2 to 4 minutes. Subsequently, the sample was cooled down rapidly to room temperature at a cooling rate of 3 ℃ s^{-1} by turning off the heating power, and then it was taken out for characterization.

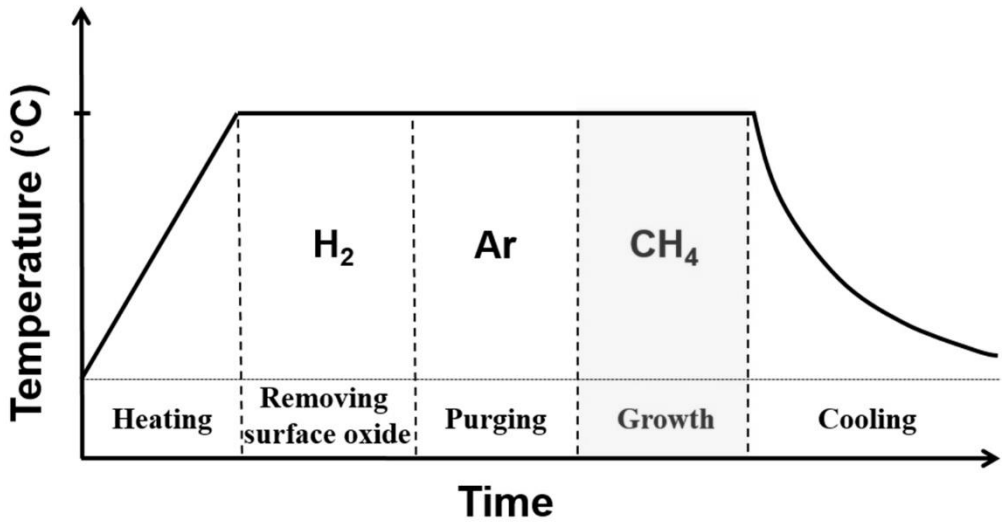

Figure 3. 1. Schematic procedure to grow single layer graphene on Cu foil

To evaluate quality, all the grown single layer graphene (SLG) films were transferred onto SiO_2/Si substrates by etching the Cu foil in an aqueous solution of iron chloride ($FeCl_3$). Prior to wet-etching, the surface of graphene/Cu was spin-coated with polymethyl methacrylate (PMMA: 950 A2), followed by spin-coating for 2 minutes under 2000 rpm and baking at 150 ℃ for 3 minutes. The purpose of the PMMA coating is to protect graphene films from cracks and tears during the transfer process [9]. When Cu foil was dissolved completely, the PMMA/graphene membrane was washed with deionized water and placed on the SiO_2/Si substrate. Finally the PMMA film was dissolved and removed by acetone.

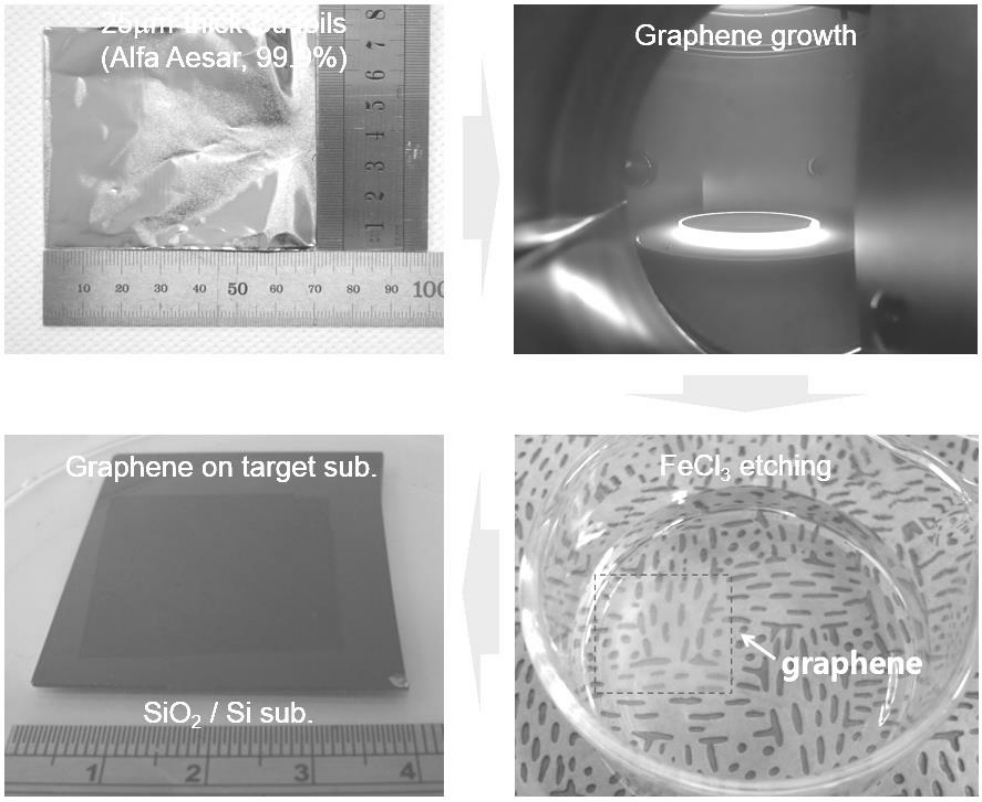

Figure 3. 2. Scheme of the sample preparation of the single layer graphene on SiO_2/Si substrate.

3.3. Characterization

The surface morphologies of graphene films on Cu substrates were analyzed by a scanning electron microscope and an optical microscope. High-resolution transmission electron microscopy (HR-TEM) studies were conducted by using a JEOL JEM-2100F. The crystallinity and the structural information of grown graphene were obtained by micro-Raman spectroscopy (Renishaw, inVia system) using a 514.5 nm laser. In order to estimate the uniformity of grown graphene, Raman spectra were collected at three different points in each graphene film. The averaged data of these points are presented in the plots of intensity ratios and the full width at half maximum (FWHM). The point-to-point variation of the Raman spectra is displayed as an error-bar. A minimal laser power of 0.75 mW was used carefully during the measurements to avoid any damage or heating of the graphene films. Electrical properties were measured using the two-probe method.

Figure 3.3a-c shows SEM images of graphene grains grown at plasma powers of 10, 50, and 170 W in Ar/CH_4 mixtures at 830 ^oC. The average grain size is ~0.4 μm when the plasma power is 10 W, but it sharply increases to ~3 μm when the plasma power is increased to 50 W. It also sharply decreased to ~0.8 μm at a plasma power of 170 W. The plot of grain size and nucleation density as a function of plasma power in Figure 3.3d shows that the grain size (the nucleation density) has a maximum (minimum) at 50 W and saturates to ~0.8 μm (~1.8 μm^{-2}) when the plasma power is higher than 120 W. This result is due to the increased amount of hydrogen species at higher plasma power. It is well known that the hydrogen strongly affects the resulting grain size because of its dual role in graphene growth; an activator of CH_x radicals into more active species ($CH_x + H \leftrightarrow CH_{x-1} + H_2$) and an etching reagent of graphene (H + graphene ↔ (graphene - C) + CH_x) [18]. These two processes compete and affect the growth of graphene depending on the partial pressure of hydrogen. The increase of grain size at low plasma power (10–50 W) is due to the co-catalytic role of hydrogen in graphene growth. On the other hand, the reduced grain size at higher plasma power (> 50 W) can be attributed to the etching effect of the graphene by hydrogen. A SEM image of the graphene grains grown at plasma power of 50 W is shown in Figure 3.3b. The

resulting grain size and nucleation density is plotted in Figure 3.3d

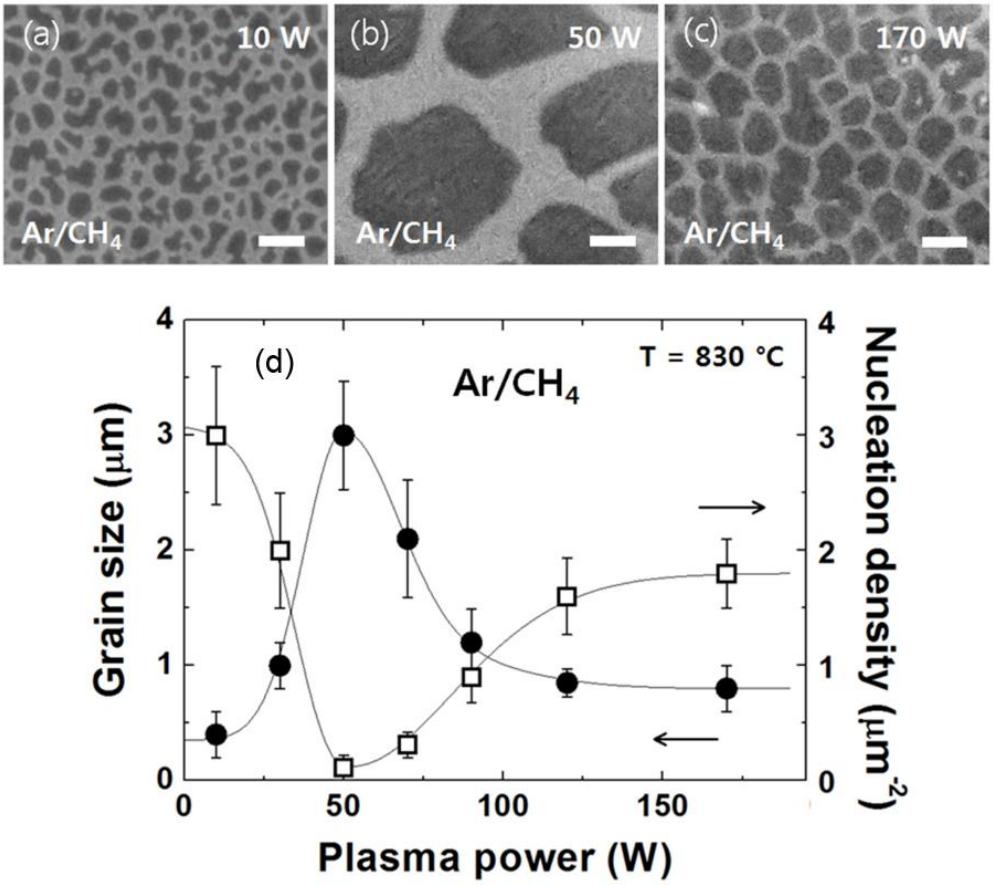

Figure 3. 3. SEM images of graphene grains grown (a, b) for 1 minute at plasma powers of 10, 50 W and (c) for 20 seconds at 170 W with Ar/CH_4 mixtures. Scale bar = 1 μm. (d) Grain size (filled circles) and nucleation density (open squares) of graphene as a function of plasma power under different gas mixtures.

The effect of substrate temperature on graphene growth in Ar/CH_4 condition is investigated in a temperature ranging from 700 to 830 ℃ while the plasma power and the growth time were maintained at 50 W and 3 minutes, respectively. Figure 3.4a shows Raman spectra of graphene film grown at different substrate temperatures. As the temperature decreases, the ratio of I_D/I_G increases from 0.2 to 0.7 and I_{2D}/I_G decreases from 4.0 to 2.2 (Figure 3.4b). The higher intensity of the D peak and the broader FWHM of the 2D band (Figure 3.4c) at lower growth temperatures suggest that there are gradual increments of disorder for graphene grown at lower temperatures. Even at the substrate temperature of 700 ℃, however, the ratio of I_{2D}/IG is higher than 2 and a single-Lorentzian 2D peak is observed, indicating that a SLG was grown with some defects.

We further investigated the Raman spectra of graphene grown at 830 ^oC with Ar/CH_4 (40:1) mixtures for various growth times with a plasma power of 50 W. Figure 3.5 shows that coverage of graphene did not affect the Raman spectra. However, more than 3 minute is needed to grow fully covered graphene as shown in Figure 3.6.

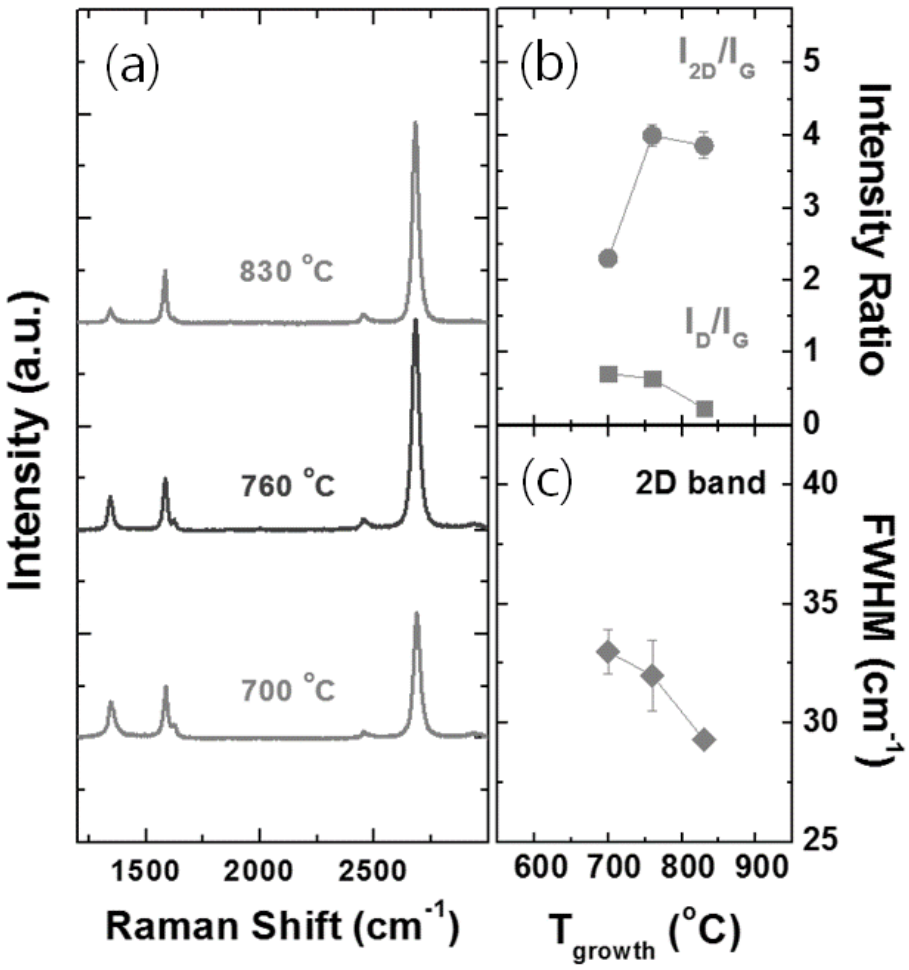

Figure 3. 4. Raman spectra of graphene films on SiO_2/Si substrate grown for 3 min at various temperatures with a plasma power of 50 W. (b) Intensity ratios of the D and 2D peaks to the G peak. (c) FWHM of 2D band of grown graphene.

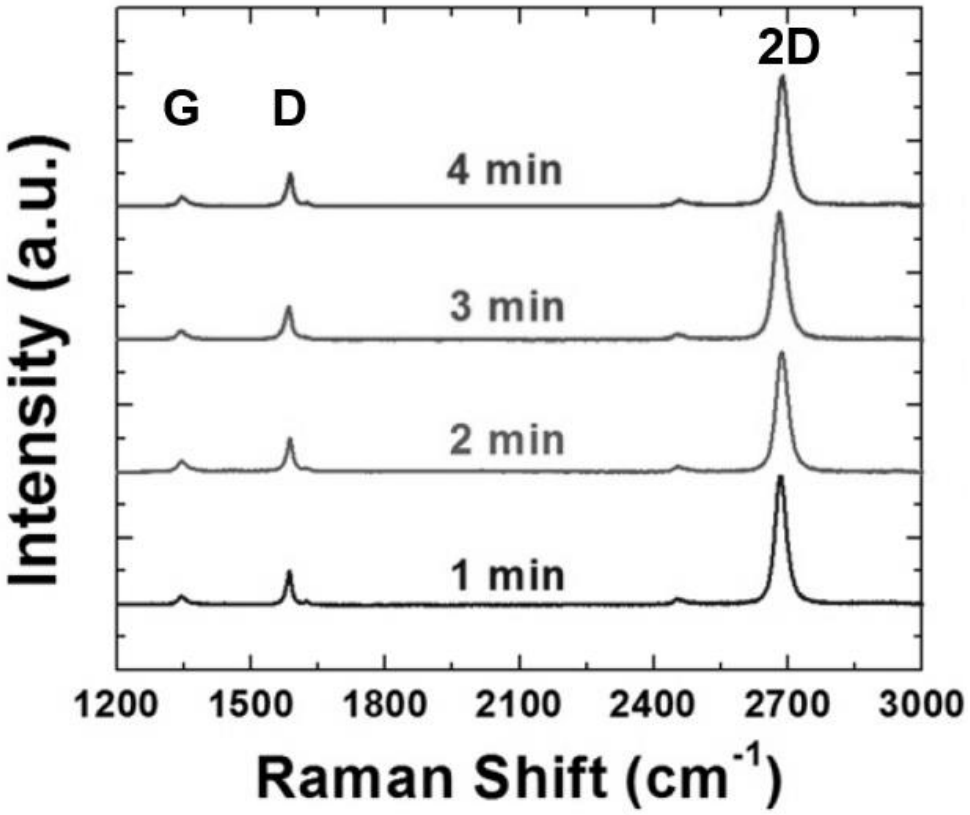

Figure 3. 5. Raman spectra of graphene grown at 830 ^{o}C with Ar/CH_4 (40:1) mixtures for various growth times with a plasma power of 50 W

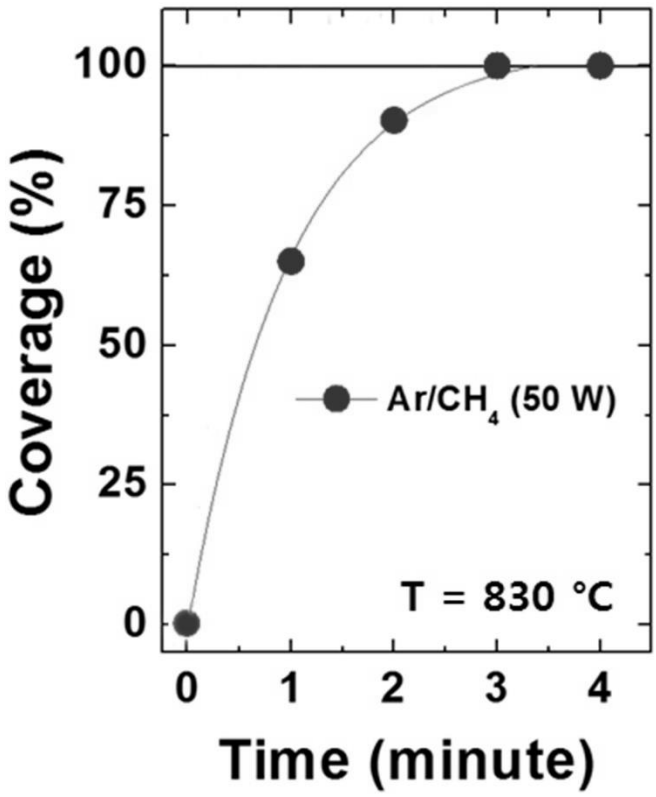

Figure 3. 6. Graphene coverage on Cu foil as a function of growth time in Ar/CH_4 gas mixtures with a plasma power of 50W, which was grown at 830 ^oC in 3 minutes.

UV-vis spectra photometer (Carry 5000, Varian) was utilized to test transmittance of SLG. SLG films on Cu foils were transferred onto double side polished (DSP) sapphire substrate to measure transmittance at the range of 200 ~ 800 nm wavelength. Then, SLG films were fabricated by O_2 plasma treatment to measure sheet resistance. Here, 4 point-probe measurement was performed with hall-bar shaped graphene patterns. As a result, SLG film showed good transmittance of larger than 90% for wavelengths ranging from 200 to 800 and 600 ohm/sq. per single graphene layer.

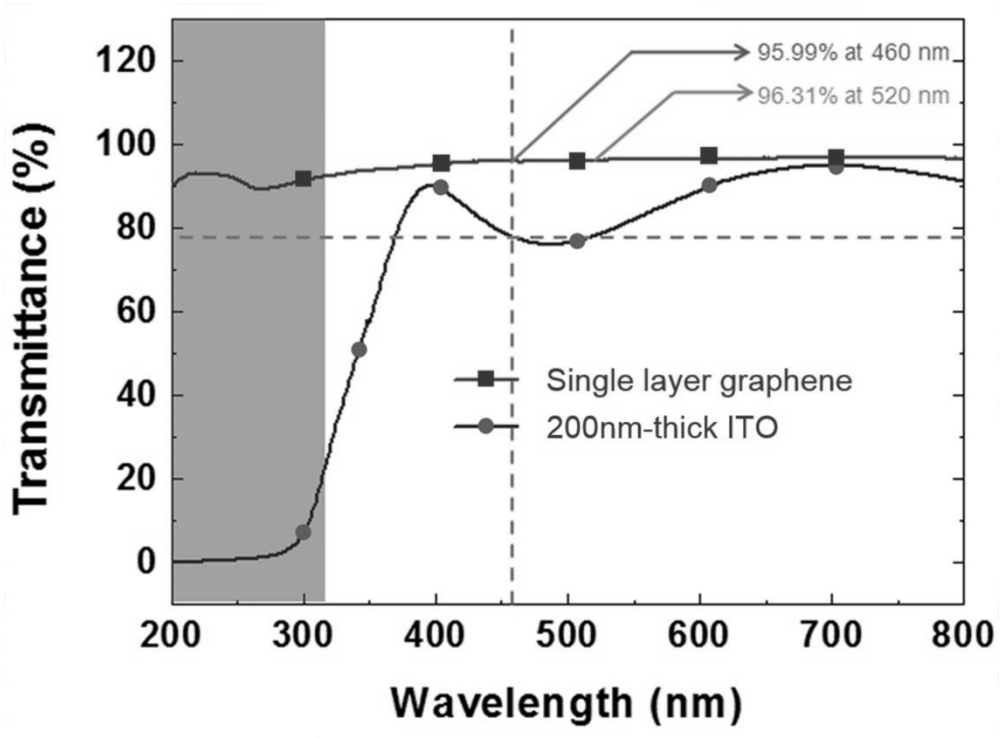

Figure 3. 7. Transmittance of SLG and 200nm-thick ITO films on DSP substrate measured in the range of 200 ~ 800 nm wavelength

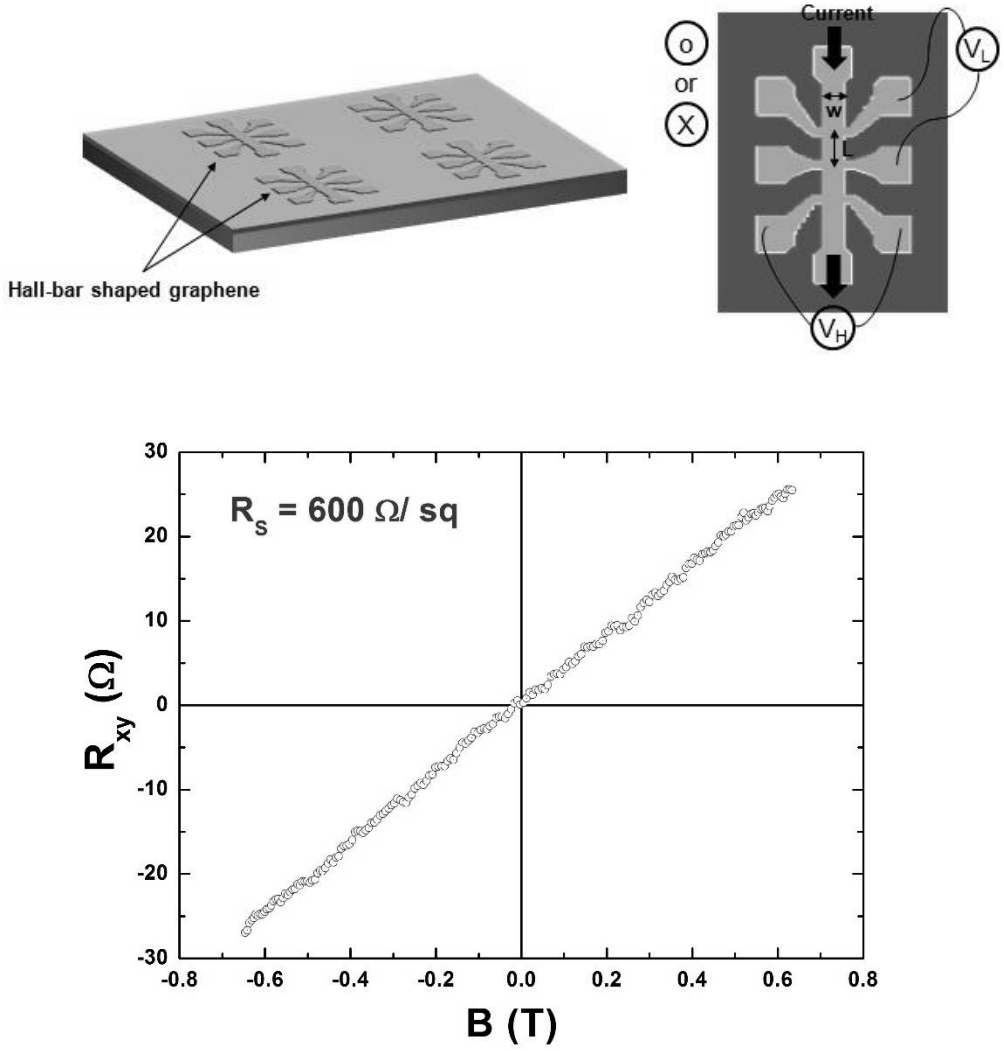

Figure 3. 8. Hall-bar shaped graphene and sheet resistance of SLG film

3.5. Reference

[1] K. S. Novoselov, A. K. Geim, S. V. Morozov, D. Jiang, Y. Zhang, S. V. Dubonos, I. V. Grigorieva and A. A. Firsov, *Science* **306**, 666-669 (**2004**).

[2] I. Meric, M. Y. Han, A. F. Young, B. Ozyilmaz, P. Kim and K. L. Shepard, *Nat Nanotechnol* **3**, 654-659 (**2008**).

[3] Y. B. Zhang, Y. W. Tan, H. L. Stormer and P. Kim, *Nature* **438**, 201-204 (**2005**).

[4] J. H. Chen, C. Jang, S. D. Xiao, M. Ishigami and M. S. Fuhrer, *Nat Nanotechnol* **3**, 206-209 (**2008**).

[5] C. Lee, X. D. Wei, J. W. Kysar and J. Hone, *Science* **321**, 385-388 (**2008**).

[6] D. V. Kosynkin, A. L. Higginbotham, A. Sinitskii, J. R. Lomeda, A. Dimiev, B. K. Price and J. M. Tour, *Nature* **458**, 872-876 (**2009**).

[7] C. Berger, Z. M. Song, X. B. Li, X. S. Wu, N. Brown, C. Naud, D. Mayou, T. B. Li, J. Hass, A. N. Marchenkov, E. H. Conrad, P. N. First and W. A. de Heer, *Science* **312**, 1191-1196 (**2006**).

[8] G. Eda, G. Fanchini and M. Chhowalla, *Nat Nanotechnol* **3**, 270-274 (**2008**).

[9] K. S. Kim, Y. Zhao, H. Jang, S. Y. Lee, J. M. Kim, K. S. Kim, J. H.

Ahn, P. Kim, J. Y. Choi and B. H. Hong, *Nature* **457**, 706-710 (**2009**).

[10] X. S. Li, W. W. Cai, J. H. An, S. Kim, J. Nah, D. X. Yang, R. Piner, A. Velamakanni, I. Jung, E. Tutuc, S. K. Banerjee, L. Colombo and R. S. Ruoff, *Science* **324**, 1312-1314 (**2009**).

[11] A. Reina, X. T. Jia, J. Ho, D. Nezich, H. B. Son, V. Bulovic, M. S. Dresselhaus and J. Kong, *Nano Lett* **9**, 30-35 (**2009**).

[12] S. J. Chae, F. Gunes, K. K. Kim, E. S. Kim, G. H. Han, S. M. Kim, H. J. Shin, S. M. Yoon, J. Y. Choi, M. H. Park, C. W. Yang, D. Pribat and Y. H. Lee, *Adv Mater* **21**, 2328-2333 (**2009**).

[13] S. F. Chichibu, A. Uedono, T. Onuma, B. A. Haskell, A. Chakraborty, T. Koyama, P. T. Fini, S. Keller, S. P. Denbaars, J. S. Speck, U. K. Mishra, S. Nakamura, S. Yamaguchi, S. Kamiyama, H. Amano, I. Akasaki, J. Han and T. Sota, *Nat Mater* **5**, 810-816 (**2006**).

[14] J. Chamings, S. Ahmed, S. J. Sweeney, V. A. Odnoblyudov and C. W. Tu, *Appl Phys Lett* **92**, 021101 (**2008**).

[15] S. I. Na, S. S. Kim, J. Jo and D. Y. Kim, *Adv Mater* **20**, 4061-4067 (**2008**).

[16] X. Wang, L. J. Zhi and K. Mullen, *Nano Lett* **8**, 323-327 (**2008**).

[17] V. C. Tung, L. M. Chen, M. J. Allen, J. K. Wassei, K. Nelson, R. B.

Kaner and Y. Yang, *Nano Lett* **9**, 1949-1955 (**2009**).

[18] I. Vlassiouk, M. Regmi, P. F. Fulvio, S. Dai, P. Datskos, G. Eres and S. Smirnov, *Acs Nano* **5**, 6069-6076 (**2011**).

Chapter 4

High performance LEDs with SLG

4.1. Fabrication-induced damages

For mesa structures, photoresist (PR) mask has been widely used to fabricate GaN-based LEDs with various transparent conducting electrodes including ITO [1, 2], Ni/Au [3] and graphene electrodes [4-6]. Naturally, for applying graphene electrodes to GaN-based high performance LEDs, many researchers employed those to avoid damages to graphene layer. However, during the LED that fabrication procedure it was found graphene electrodes were damaged from ionized plasma.

As shown in Figure 4.1, in order to confirm that the graphene was damaged by the ion bombardment during ICP GaN etching process, we prepared three types of samples as follows.

Sample #1: 3 μm thick PR (AZ 7220) coated at 2000 rpm

Sample #2: 5 μm thick PR (AZ 7220) coated at 1000 rpm,

Sample #3: 3 μm thick PR + Ti/Au (10/30 nm) metal capping layer in order to protect graphene from ion bombardment, respectively.

As a result, it was found that both graphene films on the Sample #1 and Sample #2 were severely damaged after ICP GaN etching which was confirmed by AFM measurements. Even 5 μm PR, thicker than sample #1, was not enough to protect the graphene layer. However, the graphene on the Sample #3 shown in Figure 4.1(c) with additional Ti/Au (10/30 nm) metal capping layer was not damaged and showed similar to those of as-transferred graphene (which is confirmed by AFM measurement), suggesting that the ion bombardment during harsh ICP GaN etching was responsible for the graphene damage.

Considering the result, new fabrication process was designed and experimented not to affect the graphene electrodes during the fabrication process as shown in Figure 4.2. In previous studies, many researcher transferred graphene onto target substrate to form graphene electrodes as a first step of the process. Contrarily, for our case, graphene transfer was performed after defining the mesa structure to avoid plasma-induced damage to graphene electrodes.

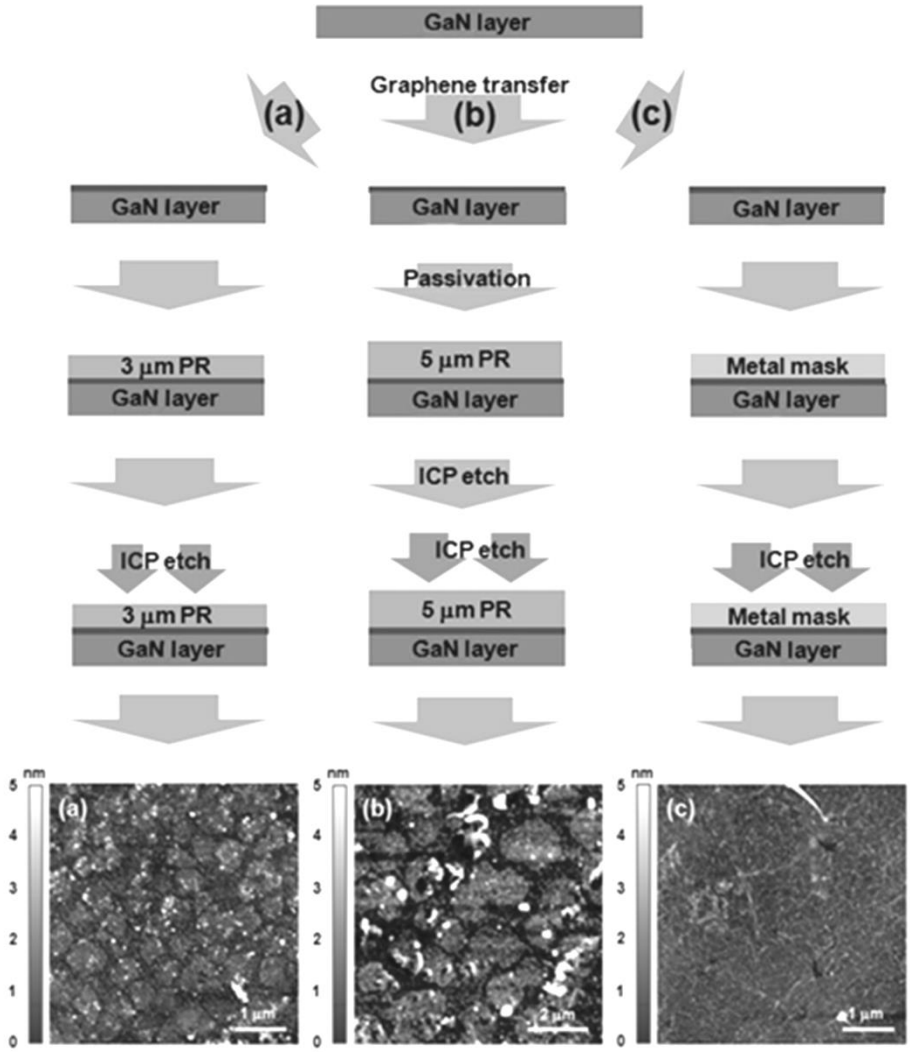

Figure 4. 1. Schematic illustration of three samples prepared for identify the origin of fabrication-related damages during the ICP etch process to form the mesa etch structure. Each sample (#1, 2, and 3) were coated with 3 um, 5 um thick PR, and metal mask to protect graphene electrodes, respectively.

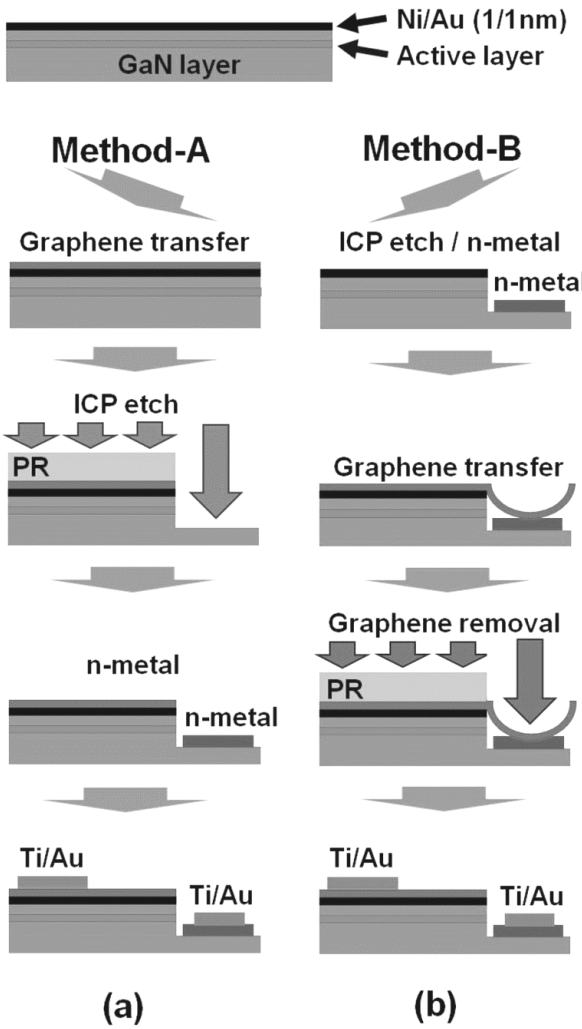

Figure 4. 2. Flow chart of newly designed graphene-LED fabrication to avoid fabrication-related damage

4.2. Experimental procedure

4.2.1. Single layer graphene (SLG) film preparation

PECVD was used with an ICP source to grow single-layer graphene on 25 μm thick polycrystalline copper (Cu) foils (Alfa Aesar, 99.9%, #13382). As above previous chapter, single layer graphene was grown at 830 ^{o}C for 3 minutes and under 50W ICP power with Ar and CH_4 gas mixture by PECVD [7].

After the growth of graphene on Cu, as-grown graphene was spin-coated with a poly-methyl methacrylate solution (PMMA, MicroChem, 950A2, 2% Solids in Anisole) at 2000 rpm for 40 s, then annealed at 150 ^{o}C for 3 min. Subsequently, the Cu was dissolved in an aqueous iron trichloride ($FeCl_3$) solution (0.1 M) for 12 h. Finally, as shown in Figure 4.2, graphene was transferred onto InGaN/GaN blue LED substrate by using conventional PMMA transfer method. After that, to remove the PMMA on top of graphene, samples were cleaned in 99.5% acetone (Samjun Chem, A1758) for 12 h.

4.2.2. LED fabrication procedure

As we assumed that process related damage to graphene electrode could be induced from LED fabrication, we prepared two types of GaN-based blue LEDs with SLG (LED-A and LED-B) made by Method-A (conventional method) [3-5, 8] and Method-B (newly designed one). For all the LED-A and LED-B, a Ni/Au (1/1 nm) layer was inserted between graphene and the p-type GaN layer to realize low contact resistant to the p-type GaN layer [9].

For Method-A, graphene was transferred onto Ni/Au (1/1 nm) layer before LED fabrication. After the transfer, a series of LED fabrication processes such as photolithography, ICP etch and, electron beam evaporation were conducted (LED-A). In contrast, for Method-B, graphene transfer was made after the ICP etch and n-type electrode formation. Then, graphene on the n-type electrode was removed by O_2 plasma etching at bias power of 50 W (LED-B). However, except for graphene transfer step, all processing conditions for each fabrication step were identical, and the final structures of LED-A and LED-B were exactly identical as illustrated in Figure 4.2 (a) and (b). As reference samples, LED-C with Ni/Au (1/1 nm) layers only was prepared for comparison with LED-A and LED-B. Similarly, LED-D with a 200 nm thick ITO layer was also prepared. Details of the fabrication procedure and light emission images of LED-C and LED-D are available in Figure 4.3 (a) and (b).

Then, ICP etch was made to expose an n-type GaN layer by using an ICP etch system (STS, Multiplex ICP system) at a bias power of 100 W. A mixed gas (Cl_2 : BCl_3 = 30 sccm : 5 sccm) was introduced during the etch process. A 3 μm thick photoresist mask (AZ Electronic Materials, AZ7220) was used to form a mesa structure. A 500 nm thick GaN layer was etched for 100 s. Subsequently, the electron beam evaporation method (ULTECH, SEE-7D series) was used to deposit a Ti/Al/Ti/Au (30/100/30/100 nm) metal layer for ohmic contact to n-type GaN, and a Ti/Au (30/100 nm) metal layer for current spreading electrodes.

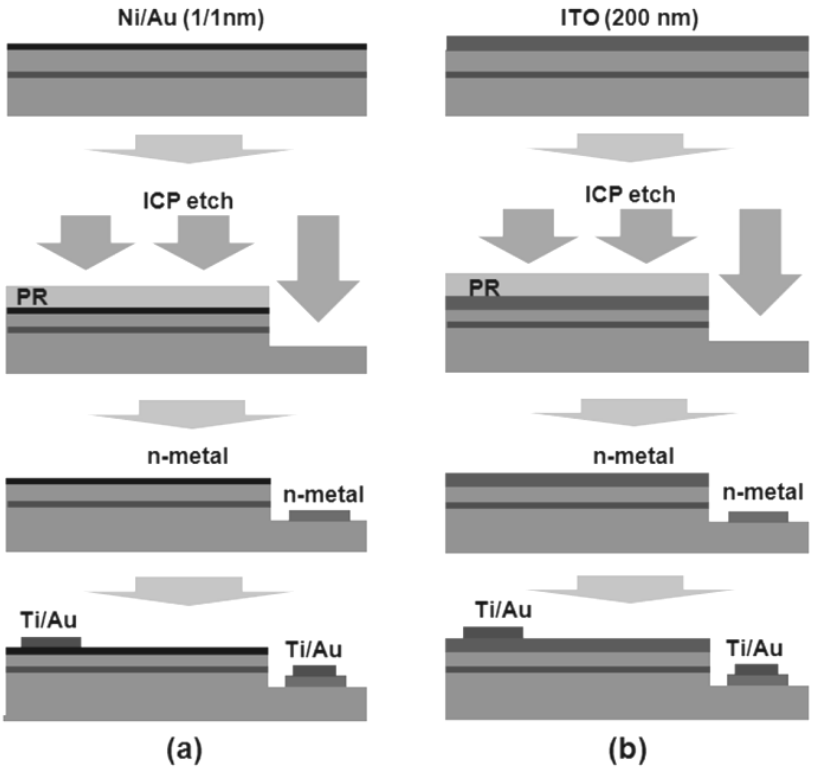

Figure 4. 3. Schematic illustration of the fabrication sequence of (a) LED-C and (b) LED-D, which were reference samples with LEDs with NiAu (1/1 nm) and 200 nm-thick ITO films, respectively.

4.3. Results and discussion

4.3.1. Performances of LEDs with graphene

Figure 4.4 and Figure 4.5 show I-V characteristics and light output power of various LEDs with single layer graphene on Ni/Au (1/1 nm) layer (LED-A and LED-B), with a Ni/Au (1/1nm) layer only (LED-C), and with a 200 nm thick ITO film (LED-D). The L-I-V characteristics and electroluminescence spectra were obtained by a Keithley 2425 source measurement unit and a Newport 1936-C spectroradiometer. In order to investigate the transmittances of a single layer graphene and a 200 nm-thick ITO film, graphene was transferred to a double-side polished (DSP) sapphire substrate, and a 200 nm thick ITO film was deposited onto DSP sapphire substrate using an e-beam evaporator, followed by rapid thermal annealing in N_2 atmosphere at 600 ℃ for 2 min. Figure 4.6 was measured using a UV-visible absorption spectrometer (Varian Carry 5000 UV-vis-near IR spectrometer). Single-layer graphene shows good transmittance greater than 90% for wavelengths ranging from 200 to 800 nm.

Note that the whole area of LED-A did not emit light uniformly as shown in Figure 4.7(a). On the other hand, the same combination of graphene and

Ni/Au (1/1 nm) layer on LED-B could spread the current uniformly to p-GaN, as shown in Figure 4.7(b). The LED-C with the Ni/Au (1/1 nm) layer only did not emit the light uniformly over the entire surface as shown in Figure 4.7(c) and (d), respectively. The operating voltage 3.95 V of LED-C was much higher than those of other LEDs due to higher parasitic resistance. Despite the use of the same quality graphene and Ni/Au layer, the partial surface of LED-A emitted light as shown in Figure 4.7(a). It was speculated that the graphene electrode might be damaged during the device processing steps, presumably by ion bombardment during the harsh ICP etching of GaN.

As shown in Figure 4.4, the forward-voltage defined at an injection current of 20 mA was found to be 3.65, 3.03, 3.90 and 3.01 V, respectively. Note that the value of 3.03 V for LED-B was close to that of LED-D. Figure 4.5 shows light output power as a function of injection current. The light output power was found to be 7.72, 9.36, 6.84 and 10.15 mW at 20 mA for LED-A, LED-B, LED-C, and LED-D, respectively. The 9.36 mW light output power for LED-B was also close to that of LED-D. Forward-voltage and light output power of 3.03 V and 9.36 mW at 20 mA for LED-B shows that the LED-B outperform similar LEDs with the graphene electrode from other groups [4] [6] [9] [10].

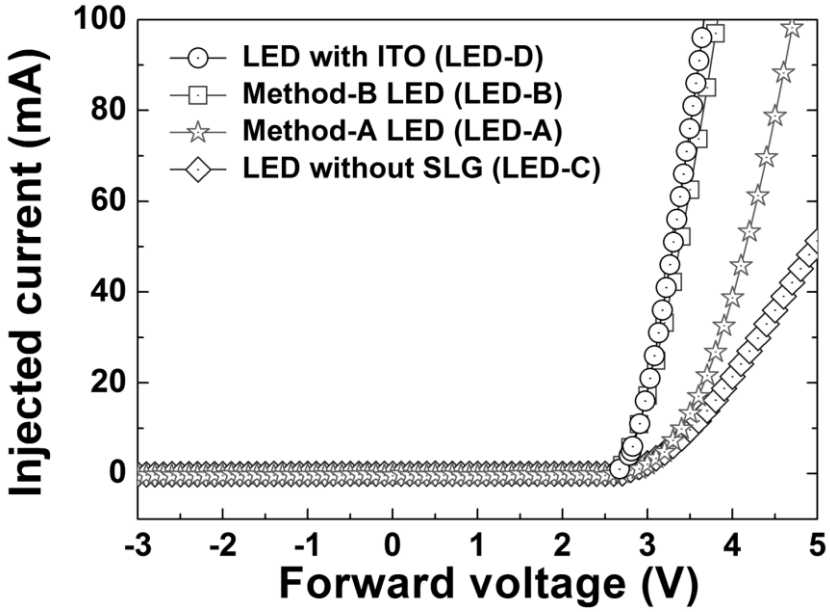

Figure 4. 4. I-V curves of LED-A and LED-B containing a SLG on a Ni/Au (1/1 nm) layer, reference LED-C with only a Ni/Au (1/1 nm) layer, and reference LED-D with 200nm-thick ITO film.

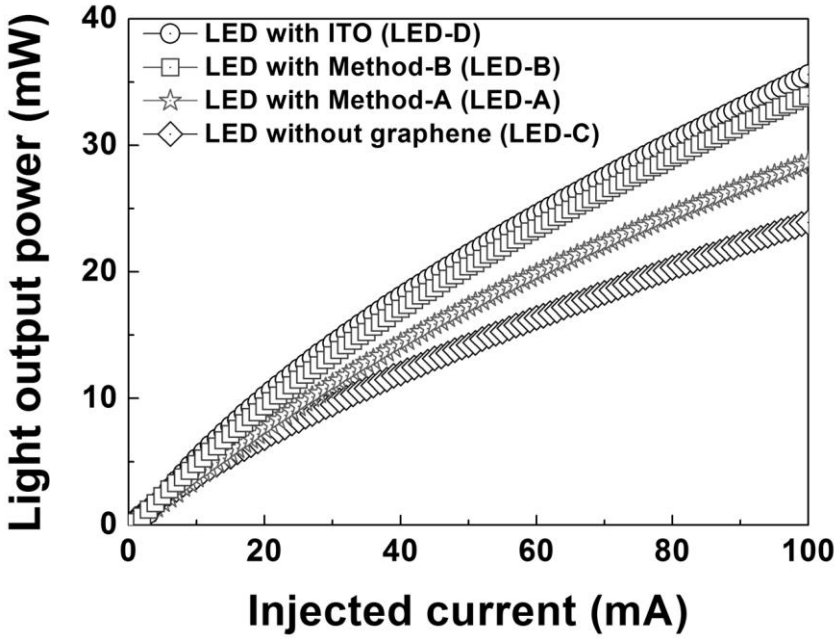

Figure 4. 5. Light output power as a function of injection current of LED-A,B,C, and –D, respectively.

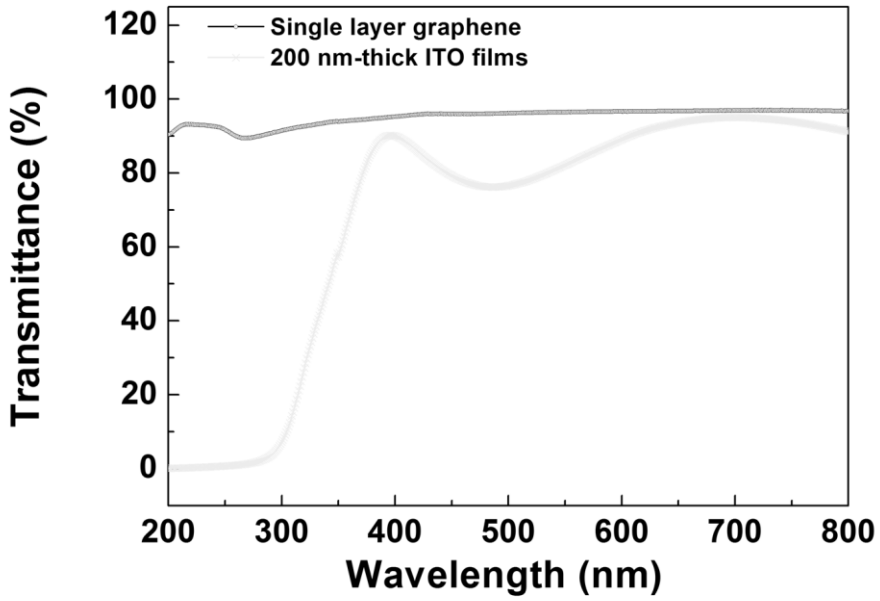

Figure 4. 6. Light output power as a function of injection current of LED-A,B,C, and –D, respectively.

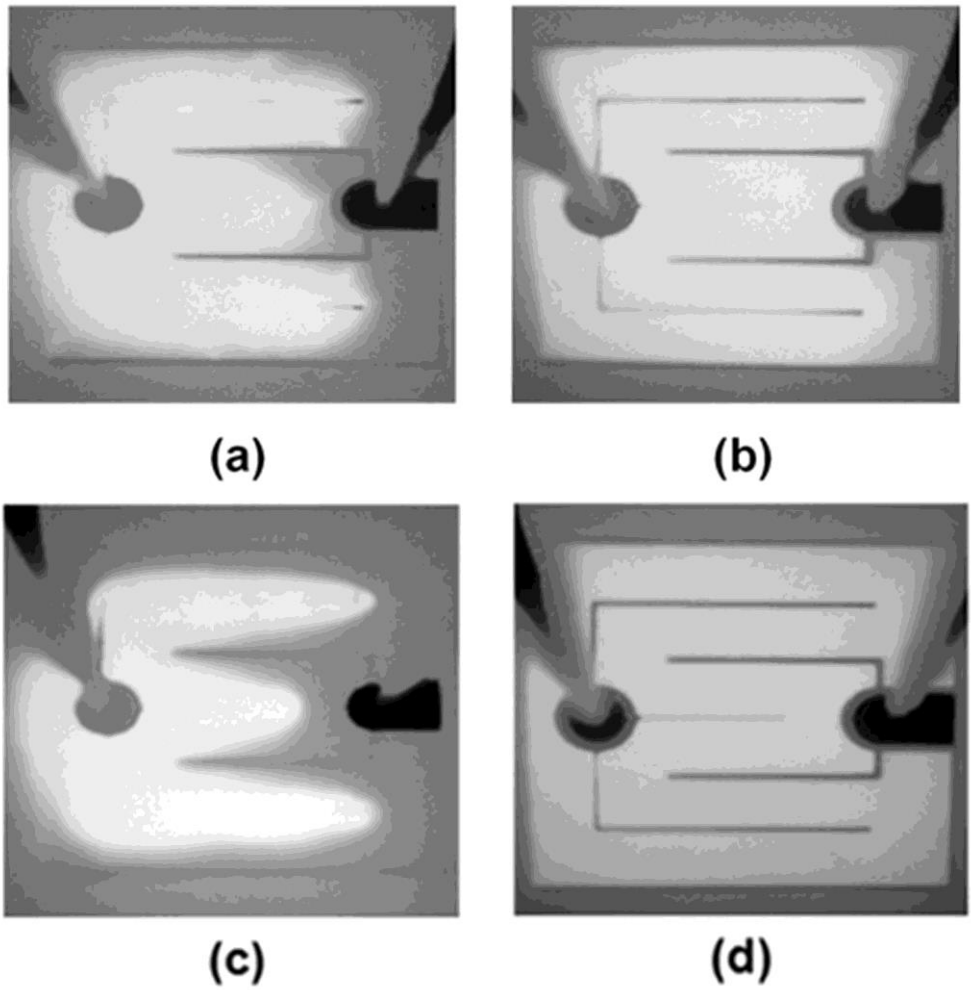

Figure 4. 7. Light output power as a function of injection current of LED-A,B,C, and -D, respectively.

4.3.2. Raman and AFM analysis

In order to estimate the quality of graphene on LED-A and LED-B fabrication, Raman spectroscopy measurement was performed using a Renishaw inVia spectroscopy system with a 514.5 nm (2.41 eV) excitation laser source. The 3.75 mW incident laser, passing through a 100x objective lens, was focused on to a spot size around 1× 1 μm^2. Raman mapping was also carried out to determine the distribution of graphene and/or carbon structure on the surface. Figure 4.8 compares Raman spectra from the graphene on Cu foil and LED substrate. The Raman spectrum denoted that both as-grown graphene on Cu foil and as-transferred graphene were of decent quality. The two important Raman features from graphene are G band at ~ 1580 cm^{-1} and 2D band at ~ 2700 cm^{-1} [11]. It is noted that the G and 2D band appear from sp^2 carbon hexagonal bonding in graphene. Especially, the 2D band corresponds to symmetry-allowed crystalline graphene without disorder [12]. Background signal from the InGaN/GaN LED substrate is showed in Figure 4.9(a)

When the graphene was transferred on to InGaN/GaN LED substrate, we obtained Raman spectra with almost the same intensity ratio of the 2D band to the G band with the graphene on SiO_2 (300 nm)/Si substrate. The large 2D

band at ~ 2688 cm^{-1} could be fitted by a single Lorentzian curve with full width at half maximum (FWHM) of ~ 33 cm^{-1}. This value corresponds to monolayer graphene [11], implying that the transfer process was safely made. An AFM image of as-transferred graphene is showed in Figure 4.10(a)

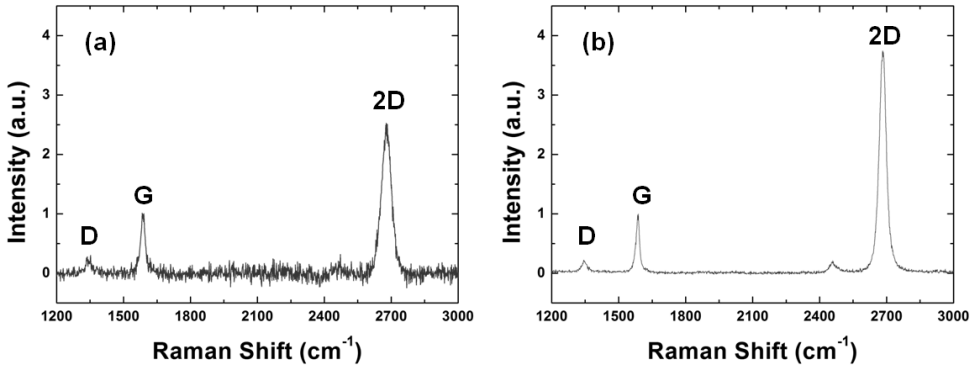

Figure 4. 8. Raman spectra of (a) as-grown single layer graphene on Cu foil, and of (b) as-tr**a**nsferred graphene on SiO_2(300 nm)/Si substrate.

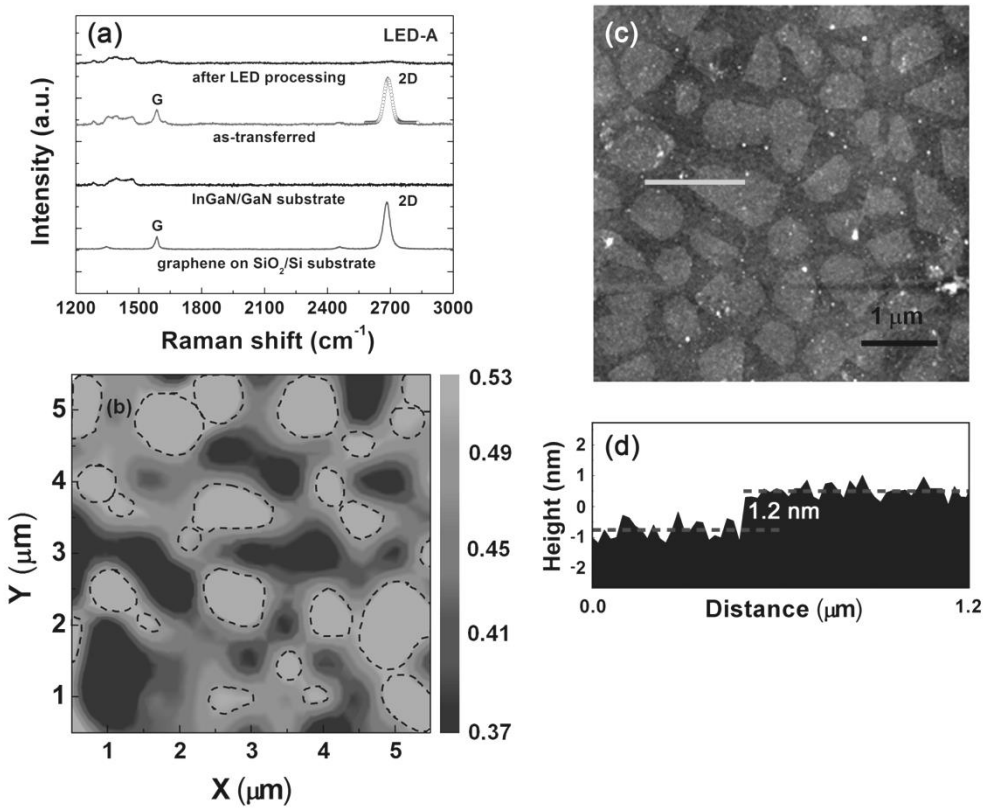

Figure 4. 9. Characterization of graphene in LED-A. (a) Raman spectra of as-transferred graphene on SiO_2 (300 nm)/Si substrate, background InGaN/GaN substrate, as-transferred on Ni/Au layer, and after LED processing, (b) Raman map of G band intensity normalized to that as-transferred to the InGaN/GaN substrate. (c) The 5 x 5 μm^2 AFM image of a graphene single layer in LED-A, and (d) height profiles along the line in the AFM image in figure 4.10(c)

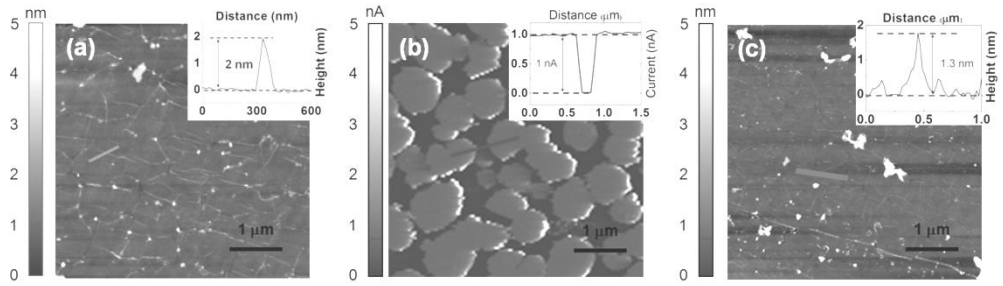

Figure 4. 10. 5 × 5 μm^2 (non-contact mode) AFM images of (a) as-transferred single layer graphene on InGaN/GaN LED substrate with inset showing height profile measured through the gray line. (b) (contact mode) current-AFM image of graphene in LED-A after LED processing with inset showing current profile measured through the black line, and (c) (non-contact mode) AFM image of graphene in LED-B with inset showing thickness profile along the gray line.

After completing LED fabrication by Method-A, however, it was found that intensities of both the G and 2D band from graphene were significantly lowered, suggesting that graphene was severely damaged during the fabrication process [12, 13]. A Raman map of the G band from graphene in LED-A was obtained as shown in Figure 4.9(b). It was found that the intensity map of the G band showed the shape of islands with a typical dimension of few submicrons, which was comparable with the typical feature sizes in the $5 \times 5\ \mu m^2$ AFM image of graphene in LED-A as in Figure 4.9(c). The height profile of an isolated graphene island is illustrated in Figure 4.9(d), where the height of 1.2 nm corresponded to the mono-layer height [14, 15]. The current-AFM result (see Figure 4.10(b)) showed that each graphene island was still conducting, whereas boundaries between graphene islands became non-conducting after LED processing. Therefore, the graphene layer made of isolated graphene islands could not spread the injection current as a transparent conducting electrode.

On the other hand, strong G and 2D bands from graphene in LED-B are observed in Raman spectra in Figure 4.11(a), after LED processing. Raman spectra from LED-B did not change much from that obtained after transfer on the InGaN/GaN LED substrate (shown in up-side line in Figure 4.11(a)). In

general, high quality monolayer graphene has a I_{2D}/I_G value higher than 2 and the FWHM of the 2D peak around ~ 33 cm^{-1}. A Raman map of I_{2D}/I_G from LED-B is shown in Figure 4.11(b). I_{2D}/I_G was higher than 1.5 over the whole $5 \times 5\ \mu m^2$ area. The AFM image of LED-B was similar to the morphology of as-transferred graphene on LED substrate (Figure 4.9(c)). These results indicate that the graphene on the surface of LED-B remained intact, suggesting that Method-B is a very effective fabrication method to reduce or avoid the process-induced damages to graphene.

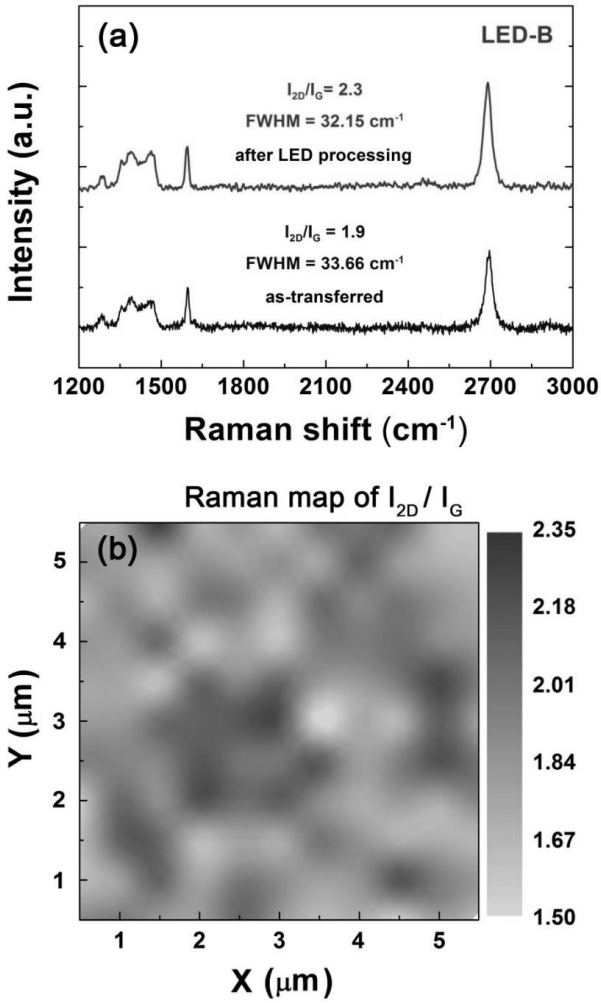

Figure 4. 11. Raman analysis of graphene in LED-B. (a) Raman spectra of as-transferred graphene in InGaN/GaN substrate (down-side) and graphene after LED processing (up-side) with little change in Raman spectra, and (b) Raman map of I_{2D}/I_G from graphene in LED-B.

4.4. Reference

[1] S. M. Pan, R. C. Tu, Y. M. Fan, R. C. Yeh and J. T. Hsu, *Ieee Photonic Tech L* **15**, 649-651 (**2003**).

[2] T. Jeong, H. J. Park, J. W. Ju, H. S. Oh, J. H. Baek, J. S. Ha, G. H. Ryu and H. Y. Ryu, *Ieee Photonic Tech L* **26**, 649-652 (**2014**).

[3] S. H. Su, C. C. Hou, M. Yokoyama and S. M. Chen, *Solid State Electron* **49**, 1905-1908 (**2005**).

[4] G. Jo, M. Choe, C. Y. Cho, J. H. Kim, W. Park, S. Lee, W. K. Hong, T. W. Kim, S. J. Park, B. H. Hong, Y. H. Kahng and T. Lee, *Nanotechnology* **21**, 175201 (**2010**).

[5] T. H. Seo, K. J. Lee, T. S. Oh, Y. S. Lee, H. Jeong, A. H. Park, H. Kim, Y. R. Choi, E. K. Suh, T. V. Cuong, V. H. Pham, J. S. Chung and E. J. Kim, *Appl Phys Lett* **98**, 251114 (**2011**).

[6] S. Chandramohan, J. H. Kang, Y. S. Katharria, N. Han, Y. S. Beak, K. B. Ko, J. B. Park, H. K. Kim, E. K. Suh and C. H. Hong, *Appl Phys Lett* **100**, 023502 (**2012**).

[7] Y. S. Kim, J. H. Lee, Y. D. Kim, S. K. Jerng, K. Joo, E. Kim, J. Jung, E. Yoon, Y. D. Park, S. Seo and S. H. Chun, *Nanoscale* **5**, 1221-1226 (**2013**).

[8] H. K. Cho, J. Jang, J. H. Choi, J. Choi, J. Kim, J. S. Lee, B. Lee, Y. H. Choe, K. D. Lee, S. H. Kim, K. Lee, S. K. Kim and Y. H. Lee, *Opt Express* **14**, 8654-8660 (**2006**).

[9] J. M. Lee, H. Y. Jeong, K. J. Choi and W. Il Park, *Appl Phys Lett* **99**, 041115 (**2011**).

[10] S. Chandramohan, J. H. Kang, Y. S. Katharria, N. Han, Y. S. Beak, K. B. Ko, J. B. Park, B. D. Ryu, H. K. Kim, E. K. Suh and C. H. Hong, *J Phys D Appl Phys* **45**, 145101 (**2012**).

[11] A. C. Ferrari, J. C. Meyer, V. Scardaci, C. Casiraghi, M. Lazzeri, F. Mauri, S. Piscanec, D. Jiang, K. S. Novoselov, S. Roth and A. K. Geim, *Phys Rev Lett* **97**, 187401 (**2006**).

[12] M. A. Pimenta, G. Dresselhaus, M. S. Dresselhaus, L. G. Cancado, A. Jorio and R. Saito, *Phys Chem Chem Phys* **9**, 1276-1291 (**2007**).

[13] A. C. Ferrari, *Solid State Commun* **143**, 47-57 (**2007**).

[14] K. S. Kim, Y. Zhao, H. Jang, S. Y. Lee, J. M. Kim, K. S. Kim, J. H. Ahn, P. Kim, J. Y. Choi and B. H. Hong, *Nature* **457**, 706-710 (**2009**).

[15] Y. Y. Wang, Z. H. Ni, T. Yu, Z. X. Shen, H. M. Wang, Y. H. Wu, W. Chen and A. T. S. Wee, *J Phys Chem C* **112**, 10637-10640 (**2008**).

Chapter 5

LEDs with directly grown graphene

5.1. Introduction

Graphene is an exciting material with a great potential for next-generation electronics and optoelectronics due to its excellent electrical, optical, and mechanical properties [1-3].

Currently, for device applications, large-area graphene films are grown by CVD at elevated temperatures (~1,000 ℃) on polycrystalline metal surfaces [4-6]. However, metal catalysts and high growth temperature have hindered the realization of directly integrated graphene devices due to the complicated post-growth etching/transfer process and thermal degradation of devices [6, 7]. Thus, to achieve direct integration of graphene into devices, graphene has to be grown without metal catalyst at reduced growth temperature [8]. Recently, the metal-catalyst-free growth of graphene has been tried by thermal CVD, but the high growth temperature of 1100–1600 ℃ limited its application in optoelectronic devices. Furthermore, considering that ohmic contact is

critical for full performance of the devices, ohmic contact formation between directly grown graphene (DG) and devices should be required. Therefore, in addition to reducing the growth temperature, finding methods to form ohmic contact between graphene and device is imperative to integrate graphene directly into optoelectronic devices.

Here, we demonstrate direct integration of polycrystalline graphene into GaN-based LEDs by PECVD. Due to the advantage of plasma-assisted growth, the growth temperature of graphene is reduced to 600 ℃, which is low enough to prevent thermal degradation of active layers in LEDs. This method provides a benefit of in situ ohmic-contact formation between graphene and p-GaN, leading to improved performance of LEDs. In addition, it is respected that electrical properties of directly integrated LEDs will outperform those with transferred graphene (TG) electrodes. At last, compared to conventional graphene process released from metal substrate, the non-use of a metallic catalyst underneath the graphene layer is compatible with standard processes in the semiconductor industry. In other words, DG method does not require multiple process steps, including coating with organic materials for catalyst etching and transfer, photo/e-beam lithography, and wet/dry etching for the application of graphene

5.2. Experimental details

5.2.1. Direct graphene growth

SiO_2(300 nm)/n-Si substrates were mounted on the graphite holder in the growth chamber via a magnetically coupled transfer rod which is operated automatically. Prior to the graphene growth, O_2 gas was introduced into the chamber at a flow rate of 40 standard cubic centimeters per minute (sccm) and discharged at an RF power of 50 W for 3 minutes to remove any organic materials contaminating the surface of the samples. After performing the pre-cleaning step, samples were heated to the growth temperature at a heating rate of 10 ℃/min. For the graphene growth, RF plasma was generated under a continuous flow of hydrogen (H_2, 20 sccm) and methane (CH_4, 2 sccm), while the pressure was kept at 10 mTorr (inert gases, such as Ar and N_2, are not added in the mixture). The growth temperature was varied from 500 to 900 ℃. The gas mixtures were discharged at a power of 50 W for a specific growth time. Subsequently, sample was cooled to room temperature at a cooling rate of 3 ℃/s by turning off the heating power.

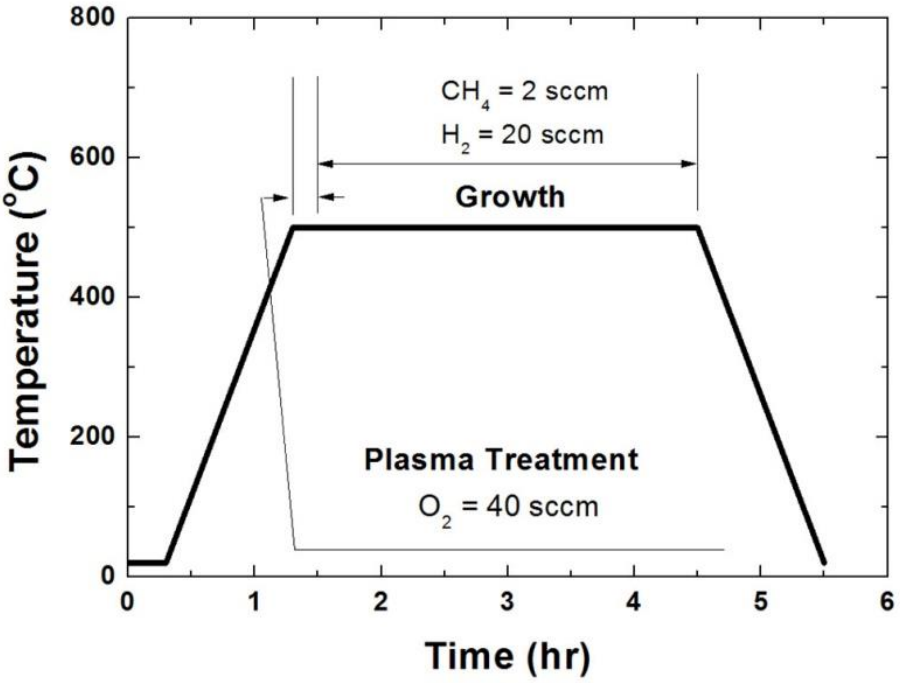

Figure 5. 1. Schematic illustration of graphene growth procedure; Temperature and gas mixture as a function of time

5.2.2. Raman spectroscopy

The growth at temperatures higher than 600 ℃ results in nanographene, as typically seen in other studies,[9-14] as evidenced by the presence of a D peak at ~1350 cm^{-1}, G at ~1580 cm^{-1}, D´ at ~1620 cm^{-1} and a small 2D at ~2680 cm^{1} (Figure 5.2). Surprisingly, there is a dramatic enhancement of 2D peak intensity as the growth temperature decreases below 600 ℃ (Figure 5.2, region II in Figure 5.3). At 500 ℃, the intensity of the 2D peak is much larger than that of the G peak, indicating the transition of nanographene to polycrystalline graphene [15, 16]. The corresponding decrease of D peak intensity is another proof of improved graphene quality. The enhancement of graphene quality at the lower growth temperature is not consistent with what we have observed in CVD graphene grown on a metallic catalyst, where better graphene films are obtained at higher growth temperatures. We note that the growth rate of graphene depends strongly on the growth temperature (Figure 5.4), which is also different from the results of CVD graphene grown on catalyst. The fast growth rate at high temperature (> 600 ℃) may cause the nucleation sites to increase too fast and lead to three-dimensional growth rather than layer-by-layer growth. On the other hand, when the temperature is lower than 500 ℃,

the growth is so slow that a continuous layer of graphene is not formed within the growth time of two hours (Figure 5.2, region I in Figure 5.3). This observation implies that the growth rate is an important factor for the growth of graphene directly on SiO_2.

The improvement of the Raman ratio of graphene grown at 500 ~ 600 ℃ can be explained as follows. The inductively coupled plasma produces a relatively high amount of atomic hydrogen which is known to etch amorphous and graphitic carbon at very different rates [17, 18]. Due to the slow growth rate, it can effectively etch amorphous carbon defect and promotes the growth of higher-quality graphene. Since the amount of atomic hydrogen is increased with the plasma power, the properties of synthesized graphene is also affected by RF plasma as shown in Figure 5.5. When the plasma power is changed from 10 to 50 W at 500 ℃ the intensity ratio of 2D peak to G peak increases from 0.9 to 1.7. However, when the plasma power is higher than 70 W, the graphene growth is forbidden because the etching rate exceeds the growth rate (Figure 5.5). These observations show the importance of fine tuning the growth parameters in catalyst-free PECVD.

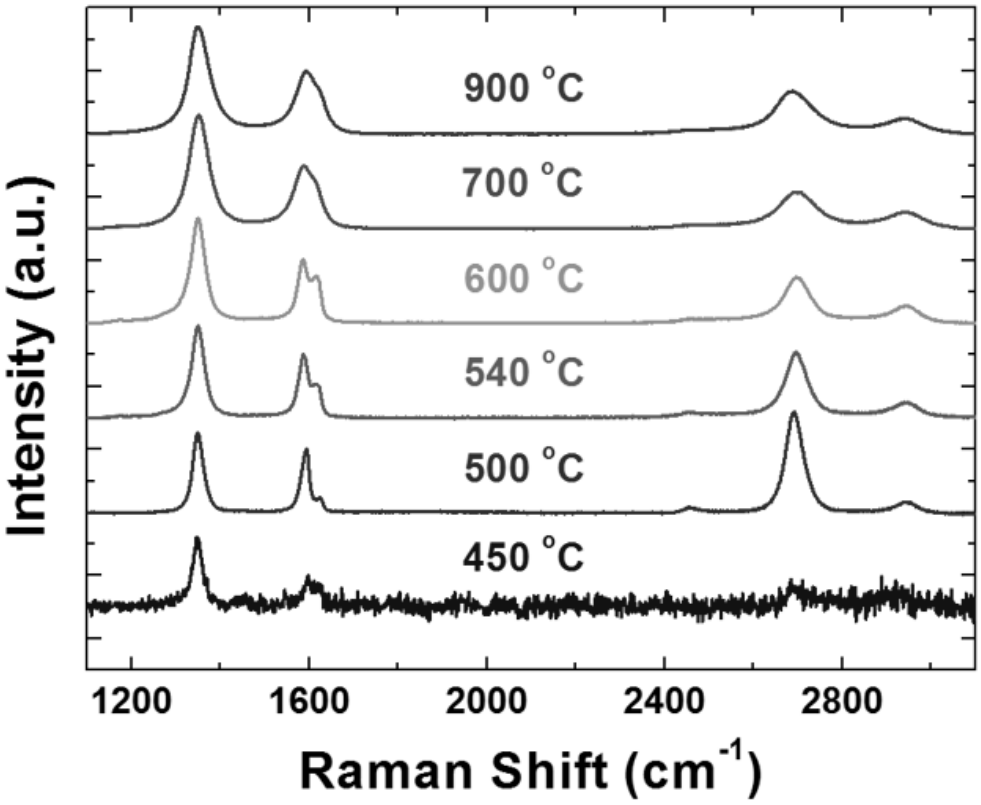

Figure 5. 2. Raman spectra grown at various temperature

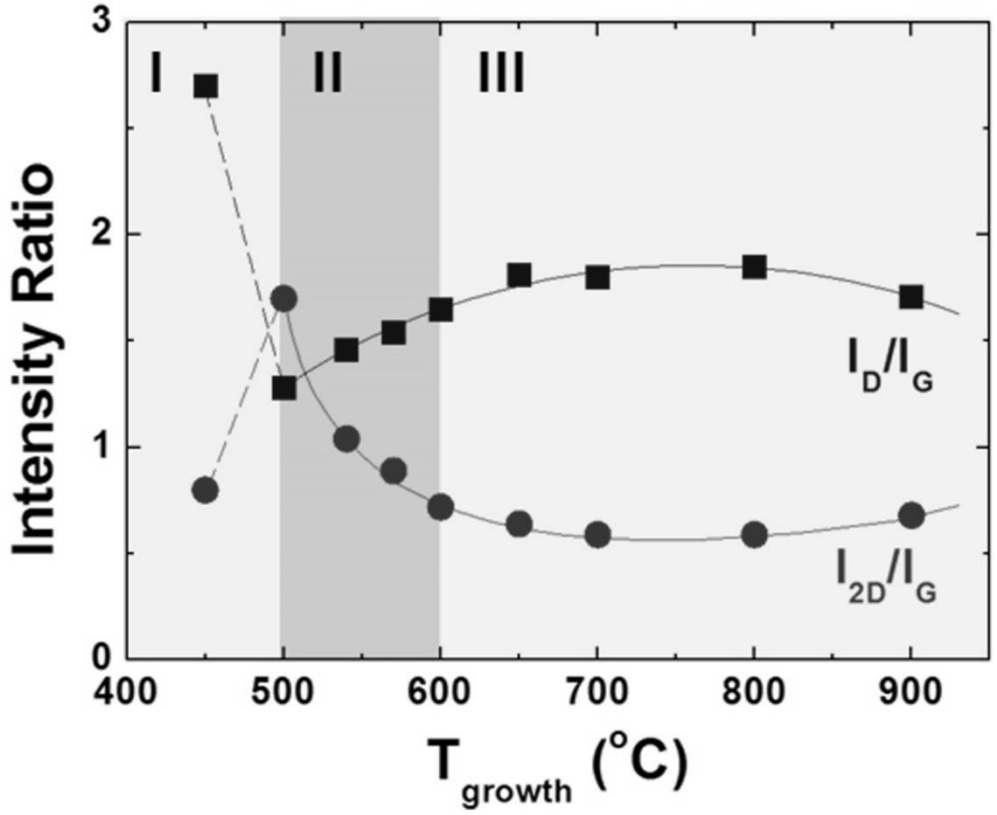

Figure 5. 3. Intensity ratios of D and 2D peaks to G peak grown at various temperature

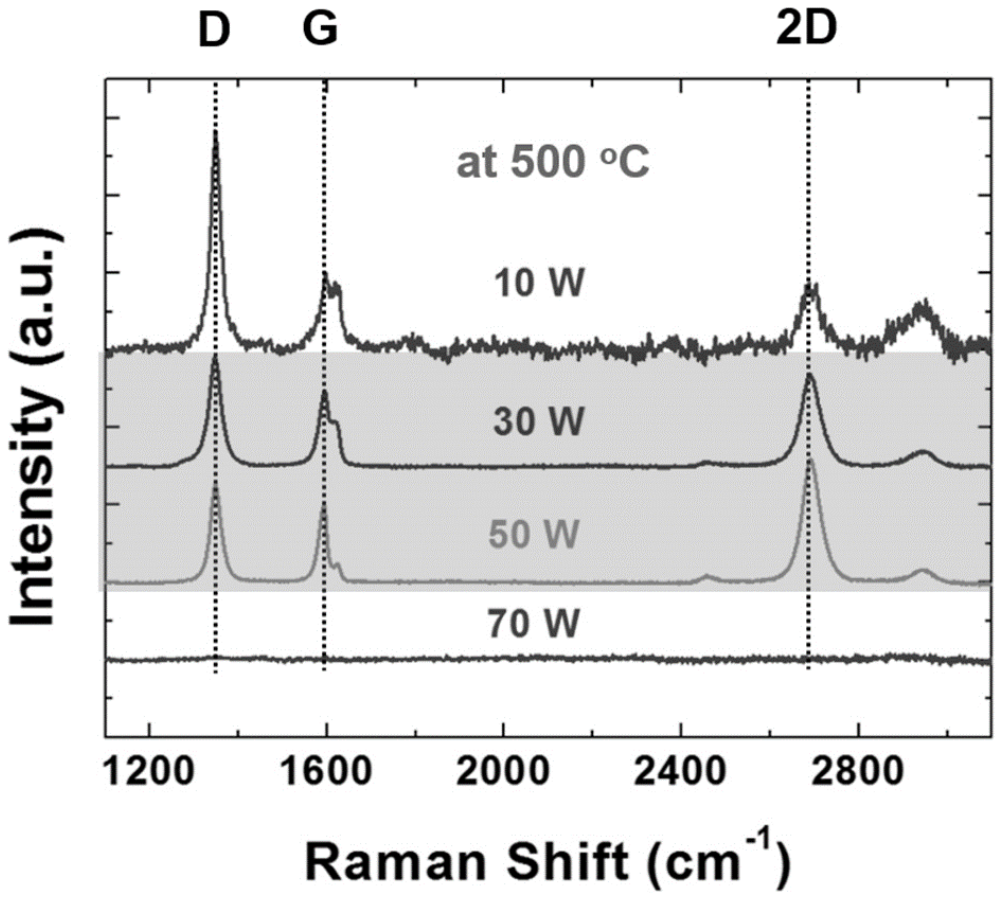

Figure 5. 4. ICP power dependency of graphene grown at 500 ºC

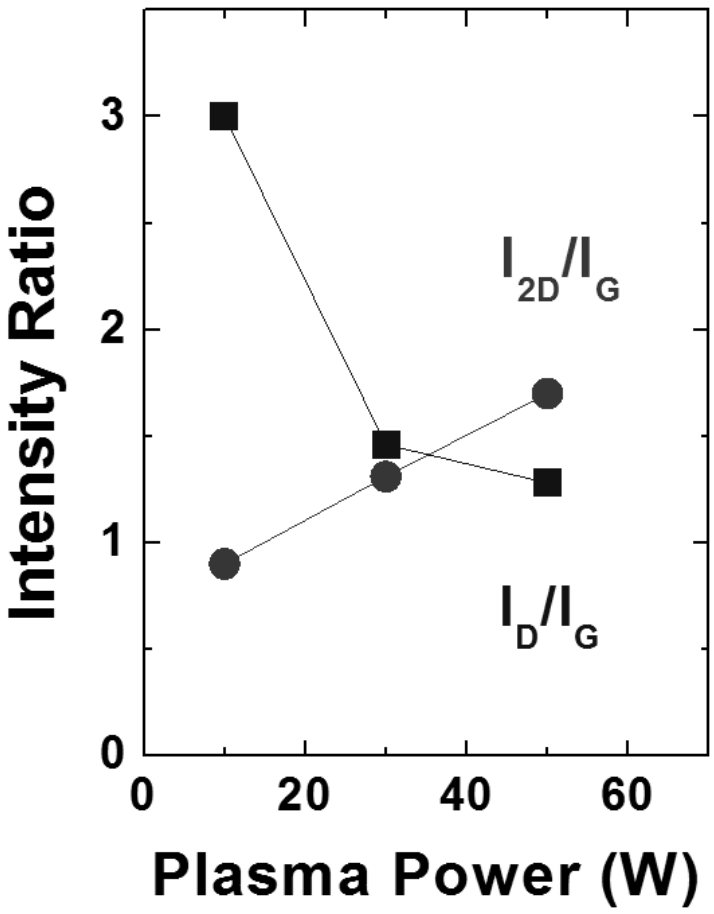

Figure 5. 5. ICP power dependency of graphene grown at 500 ºC

5.2.3. Transfer of directly grown graphene (DG) for TEM

Figure 5.6a shows the transfer process of DG onto a TEM grid. The graphene directly synthesized onto the SiO_2/Si substrate was spin-coated with PMMA (950 A2, 2% in anisole) at 2500 rpm for 30 seconds and then cured at 150 ℃ for 3 minutes. The sample was immersed in KOH solution (1M, 80 ℃) for 10 minutes. The membrane of the PMMA/graphene was peeled off from the substrate and floated to the surface of the KOH solution. It was picked up using a clean Si substrate and moved to a DI water vessel. After being washed with DI water, the membrane was transferred onto a TEM grid and dipped in acetone to remove the PMMA layer. We were able to suspend large size graphene (1.2x1.3 mm^2) on the grid as shown in Figure 5.6b.

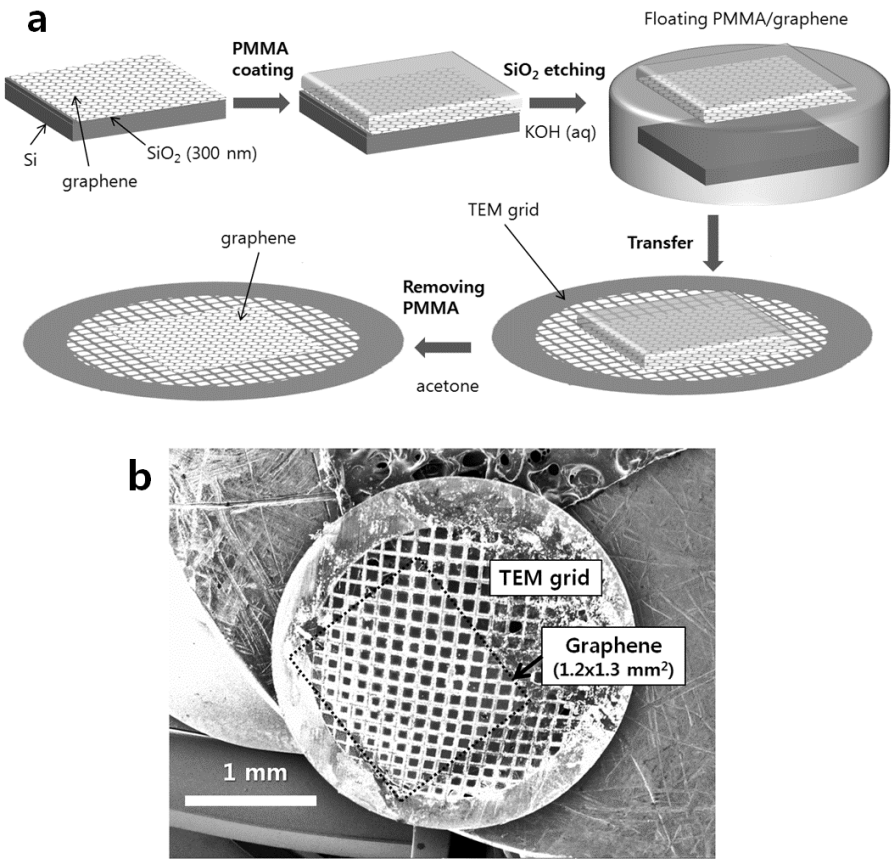

Figure 5. 6. (a) Transfer process of synthesized graphene onto a TEM grid. (b) SEM image of 1.2x1.3 mm^2 graphene transferred onto the TEM grid.

5.2.4. Structural analysis

The average thickness of graphene grown on a SiO_2 (300 nm)/Si wafer at 500 ℃ for 5 hours is about 1.2 nm, which corresponds to 3~4 layers of graphene. To further investigate the microstructure, the graphene film is transferred onto a TEM grid by etching the substrate (see Figure 5.6).

A low resolution TEM image and a selected area electron diffraction (SAED) pattern are presented at Figure 5.7 and 5.8, respectively. Considering the size of SAED aperture (~200 nm) used in our measurement, the upper limit for the crystalline domain of graphene is 200 nm in lateral size. The suspended graphene on the TEM grid is continuous over a large area as shown in Figure 5.7, and high-resolution transmission electron microscopy (HRTEM) images taken at graphene edges show successful growth of few-layer graphene with thickness variations of 1~4 layers as shown in Figure 5.8a-d.

Typical hexagonal crystalline structures are clearly observed in the selected-area electron diffraction (SAED) patterns shown in Figure 5.8e. For double layer graphene, there is a 12° rotation between the two layers, suggesting non-AA or AB-stacking as shown in Figure 5.8f. Also, randomly

stacked angles are observed in the triple and quadruple layer of graphene as shown in Figure 5.8g and h.

Atomic force microscopy (AFM) image of synthesized graphene reveals a grain size larger than 100 nm, an order of increase from the previous results as shown in Figure 5.9a [13, 14]. Each grain is coalesced into a larger one as illustrated in figure 5.9c and resulted in height variation as shown in Figure 5.9b, which corresponds to the HRTEM image in Figure 5.10.

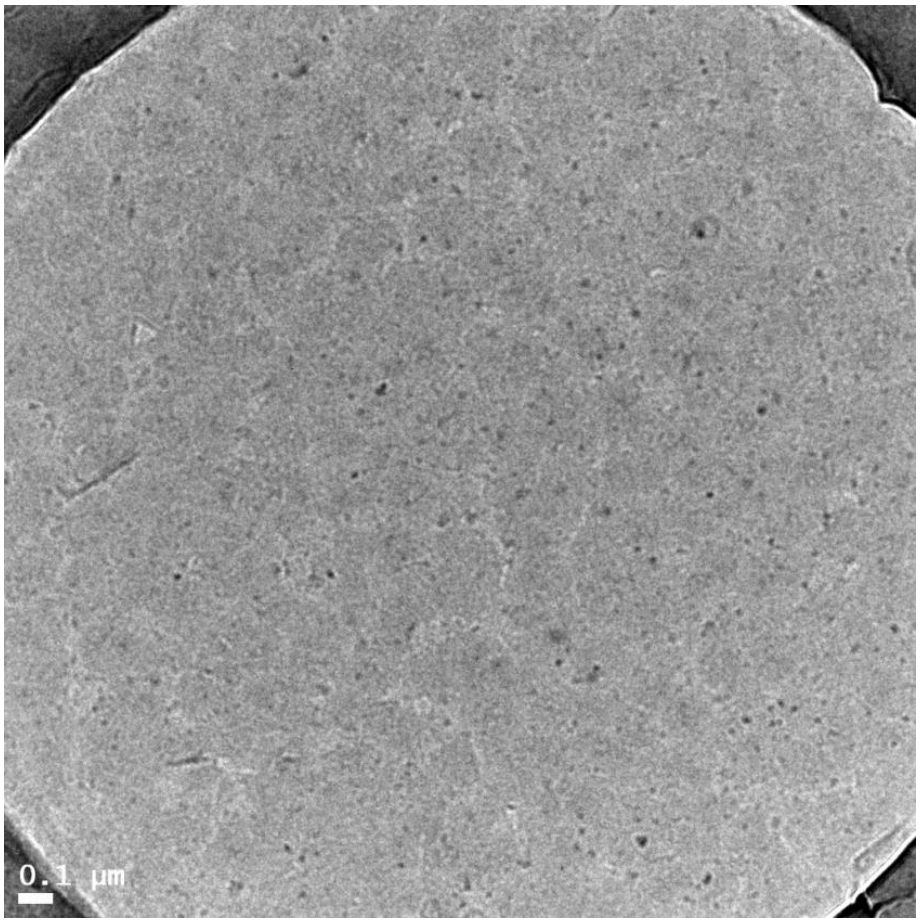

Figure 5. 7. Low-resolution TEM image of graphene film grown at 500 ℃ for 3 hours under a plasma power of 50W on SiO_2 substrate showing the film suspended on a TEM grid

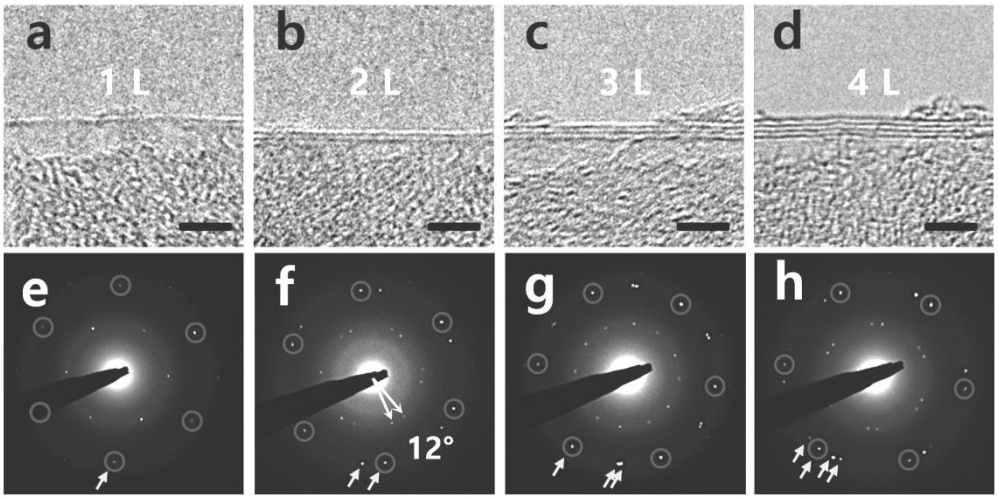

Figure 5. 8. HRTEM and SAED images of graphene film grown at 500 ℃ for 5 hours on SiO_2 substrate; (a-d) HRTEM images of graphene edges on a TEM grid, showing the thickness variation. (e-h) Hexagonal SAED patterns from honeycomb structures.

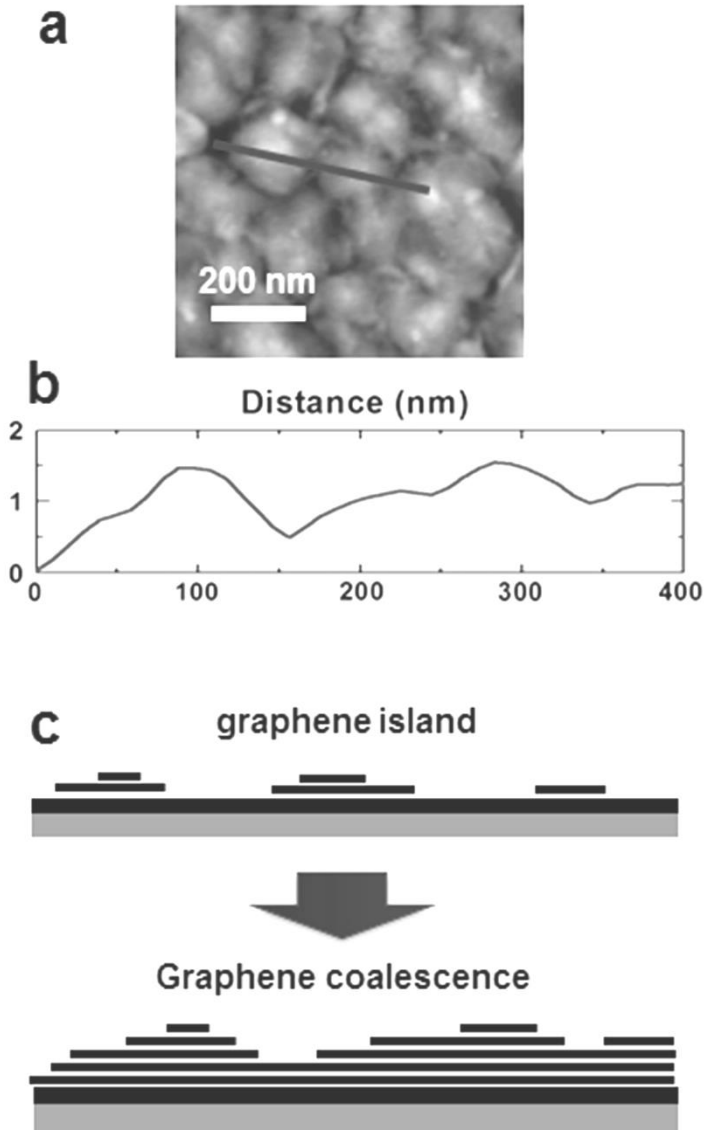

Figure 5. 9. (a) AFM image of the surface showing the grains and (b) its height profiling along with the bold line in Figure 5.8a, and (c) Schematic cross-sectional diagram

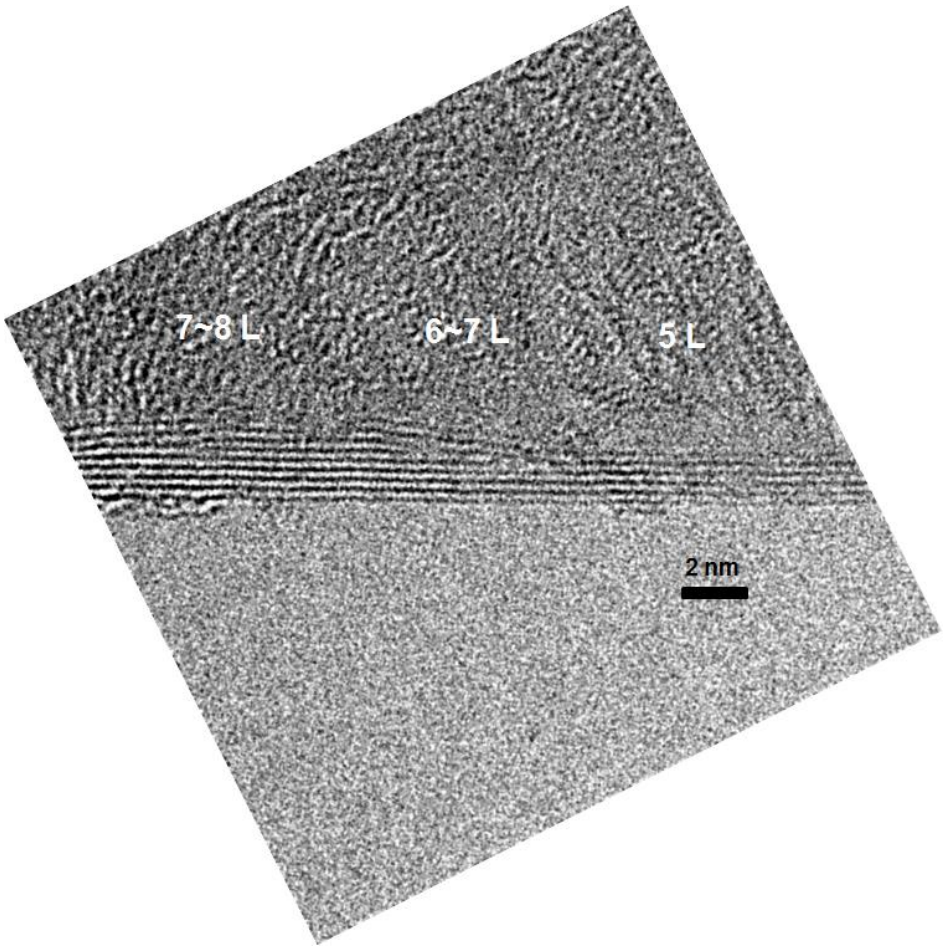

Figure 5. 10. HRTEM image of the graphene edge grown at 500 ℃ for 5 hours under a plasma power of 50W

To investigate electrical properties of polycrystalline graphene, Hall-bar shaped pattern is fabricated by using a shadow mask made of stainless steel and catalyst-free graphene growth method (see Figure 5.11). The channel width and length of Hall-bar structure is 100 μm and 300 μm, respectively.

The sheet resistance and the transmittance of graphene grown on sapphire is systematically changed as the thickness of graphene is controlled by the growth time (Figure 5.11 and 5.12). The performance as a transparent electrode is better than those of other graphene films grown directly below 1000 ℃,[13, 14] not to mention reduced graphene oxides [19].

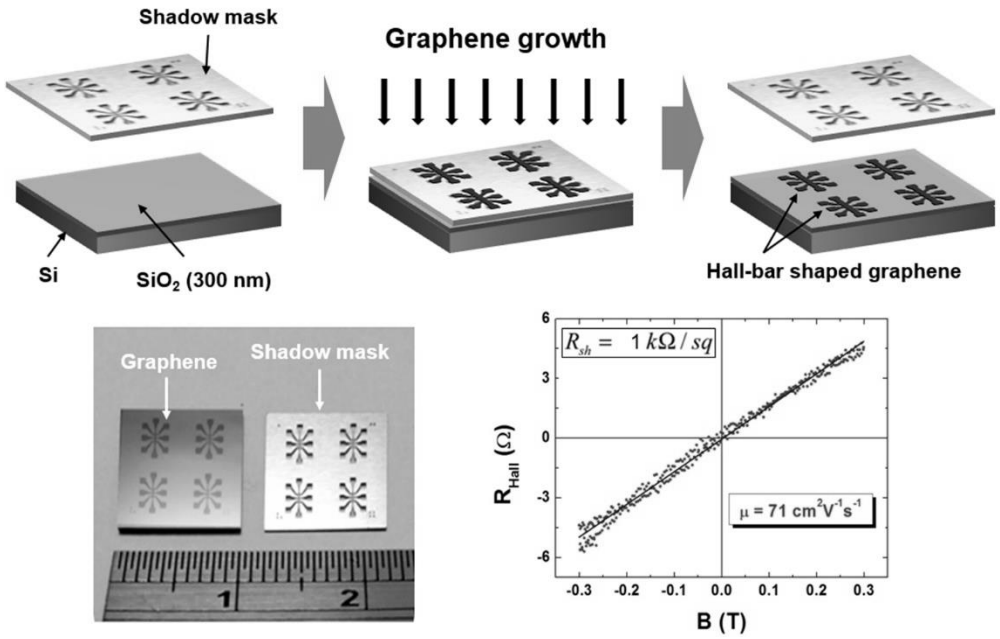

Figure 5. 11. Schematic diagram of one-tep fabrication method to obtain pre-patterned graphene on dielectric substrates without additional transfer or litho graphy process. Photograph showing the shadow mask and the graphene on SiO_2 after the growth. The mask was made of 150 μm thick stainless steel, a nd the result of hall-measurement having 1 kΩ/square sheet resistance.

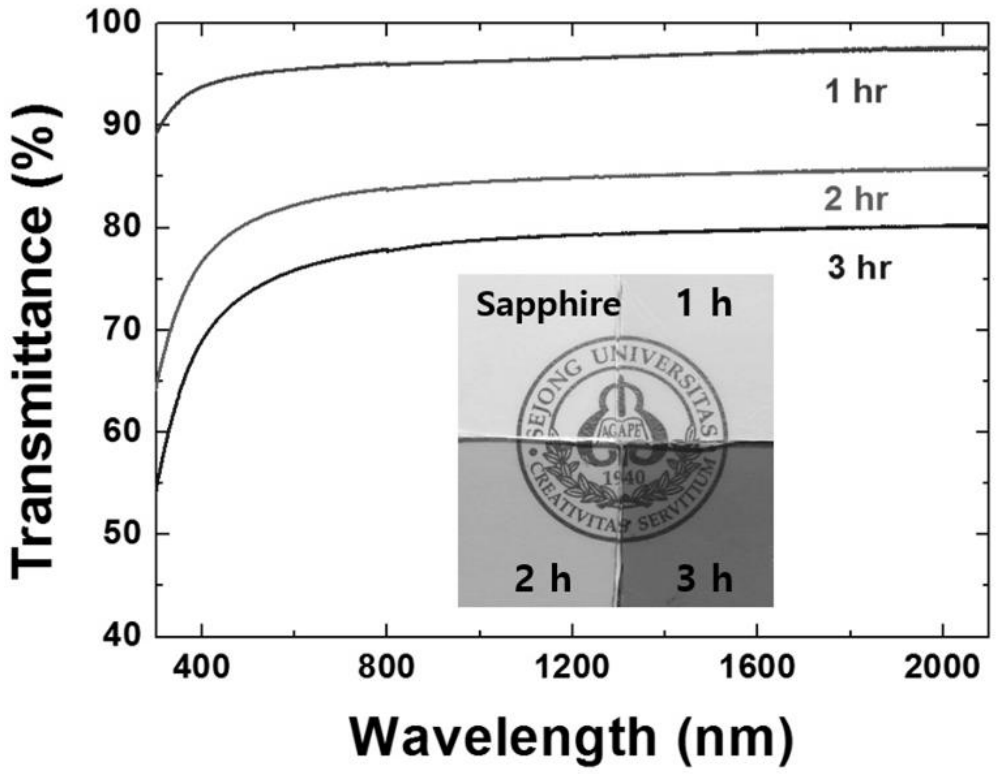

Figure 5. 12. Growth time depence of optical transmittance of the graphene films. The inset shows optical image of the graphene films grown for differenct times.

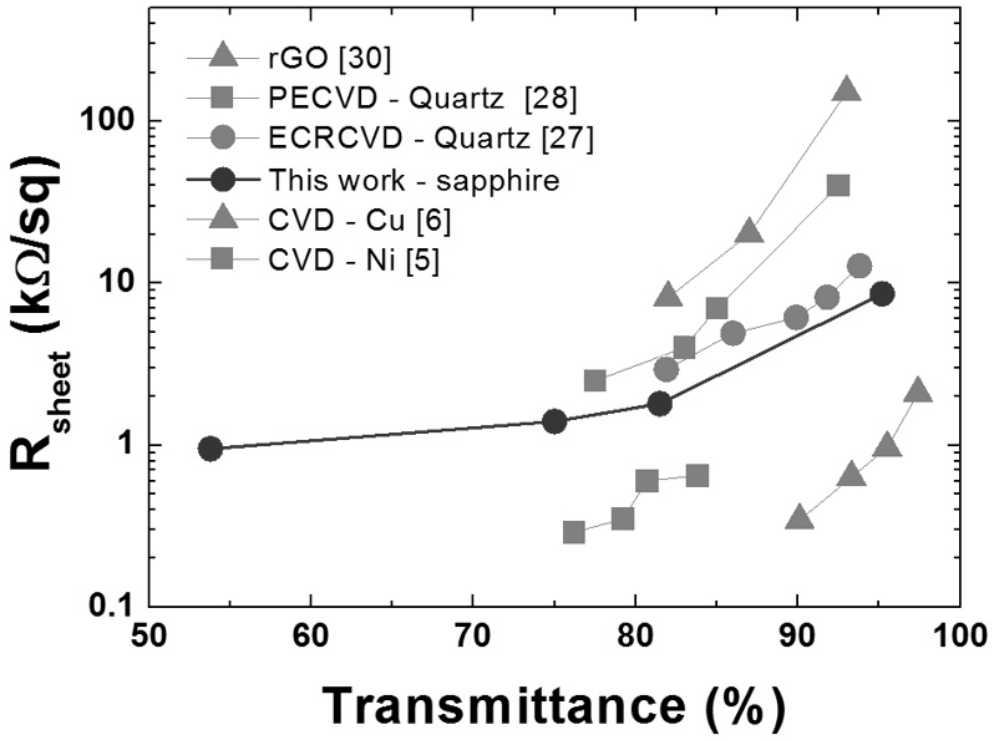

Figure 5. 13. Comparison of sheet resistance from this work and transmittance plots taken from others reported in the literature

5.2.5. Thermal degradation of InGaN/GaN multi-quantum wells

Effects of thermal damage to the properties of InGaN/GaN multi-quantum wells were investigated by using atomic force microscopy (AFM) and high-resolution X-ray diffraction (HRXRD). In order to investigate the influence to the MQWs from high temperature (~1150 ℃) at which were required to grow graphene directly on dielectric substrates in thermal chemical vapor deposition (TCVD), its structural and optical properties were measured using AFM (PSIA, XEI-100) and HRXRD (Panalytical, X'pert).

Figure S3 consists of AFM images of LED samples (a) without thermal treatment, annealed at (b) 600 ℃ and (c) 1150 ℃ for 3 hours keeping the base pressure as low as ~10^{-7} Torr. As shown in Figure 5.14a-b, with a 1 μm height valley shape and inclined terrace, average values of step distance and height are 130 nm and 0.3 nm, respectively. RMS roughness of LED sample is 0.718 nm. However, we found that thermal treatment significantly changed structural property and morphology of LED substrate (Figure 5.14c).

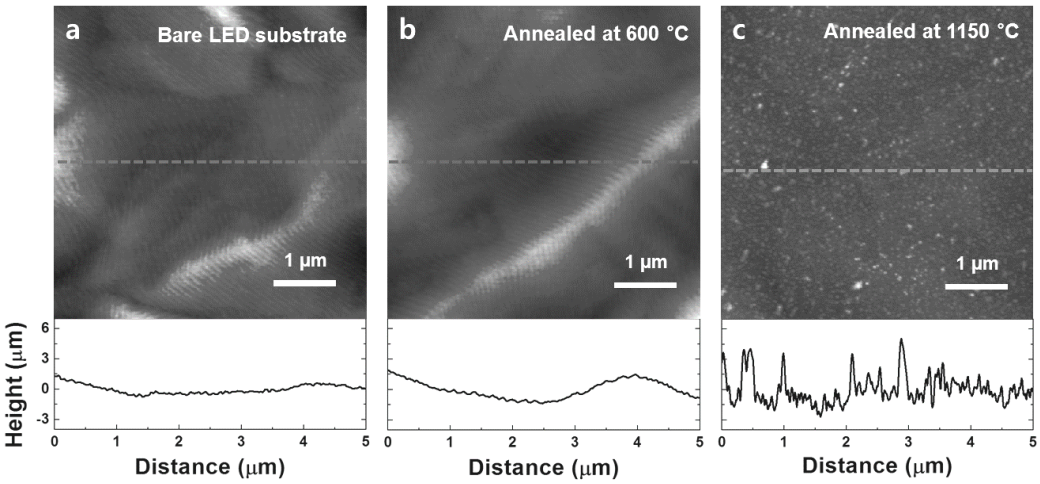

Figure 5. 14. AFM (non-contact mode) images of the samples (a) without thermal treatment and annealed at (b) 600 ℃ and (c) 1150 ℃, respectively.

Thanks to the reduced growth temperature of DG, the thermal degradation of active layer in LEDs is negligible. Figure 5.15 shows the XRD spectra of bare LED, annealed LED at 600 ℃ (our growth temperature) and 1150 ℃ (direct growth temperature in thermal CVD). In case of bare LED (up-side line of Figure 5.15), InGaN (0002) satellite peaks are observed up to the third orders which are originated from the periodicity of the InGaN/GaN multi-quantum-well (MQW) layers (see schematic diagram of the LED structure at Figure 5.16). After annealing at a temperature of 1150 ℃, only the zero-order peak is observed (middle line of Figure 5.15). The absence of higher-order peaks indicates that the MQW region is replaced by a disordered layer of InGaN through the phase separation of indium in the MQWs. However, the XRD spectrum of LED which was annealed at 600 ℃ is identical to that of bare LED spectrum, indicating that the thermal degradation of MQW layer is negligible at our growth temperature of 600 ℃ (down-side line of Figure 5.15).

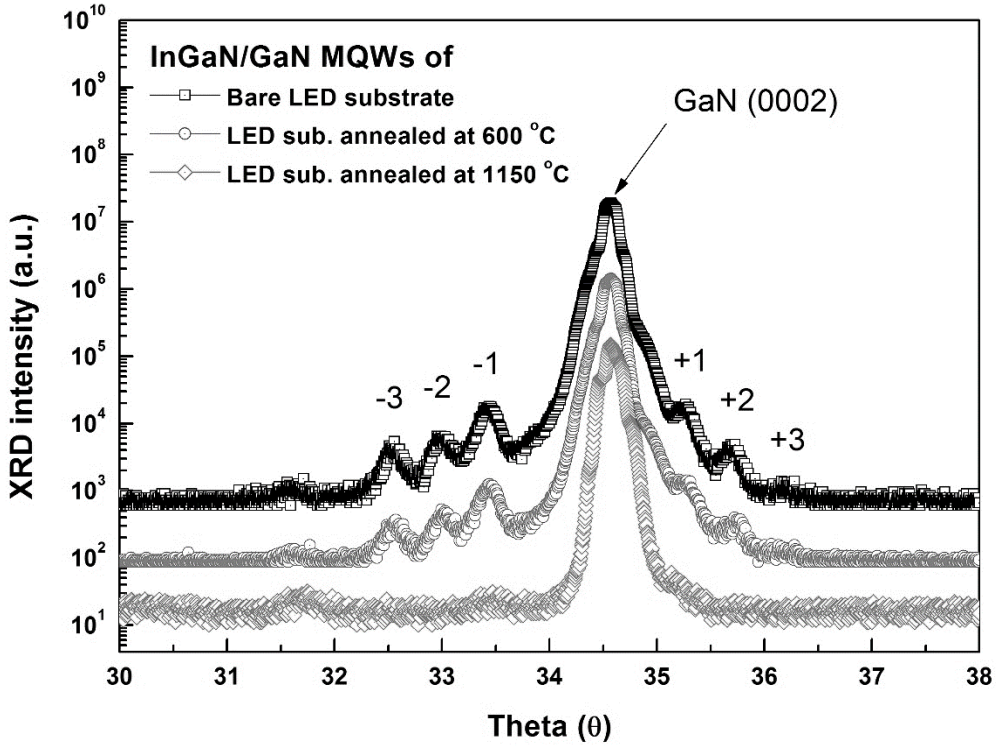

Figure 5. 15. HR-XRD curves of the InGaN/GaN MQWs before and after thermal treatment

5.2.6. Integration of graphene into LEDs

Direct growth method of graphene on LEDs enabled the transfer-free approach for the graphene-based transparent conducting electrode. We fabricated GaN-based blue LEDs with DG through a batch process for centimeter-scale LED substrates without graphene transfer process shown in Figure 5.17. Figure 5.16a-c show a schematic diagram and a scanning TEM image of LEDs with DG electrode (DG/LED), respectively. A high-magnification HRTEM image, measured at the interface of the graphene and p-GaN, clearly shows the layered structure of DG on the p-GaN surface (Figure 5.16c). Additional LEDs with transferred graphene electrode (TG/LED) is prepared by using graphene films grown on metal catalyst of Cu foil.

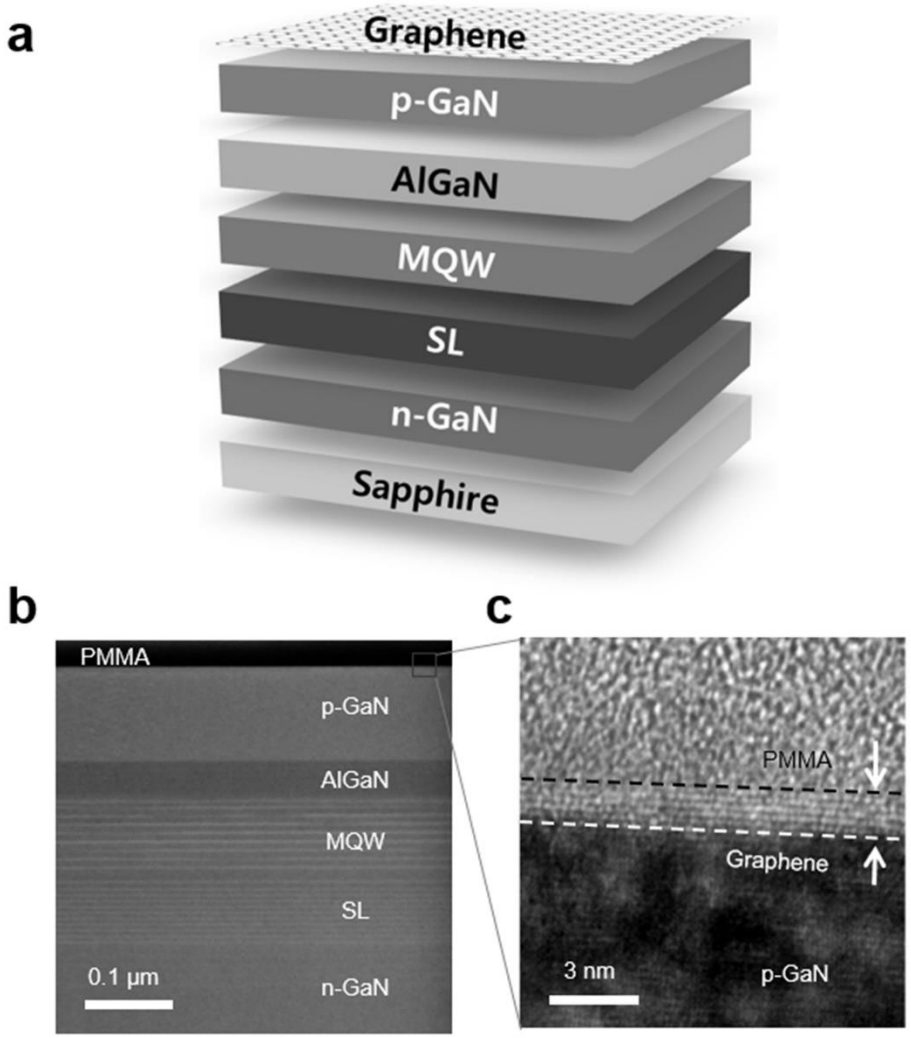

Figure 5. 16. (a) Schematic diagram and (b) scanning TEM image of the DG/LED structure. (c) HRTEM image at the interface between the p-GaN and DG electrode.

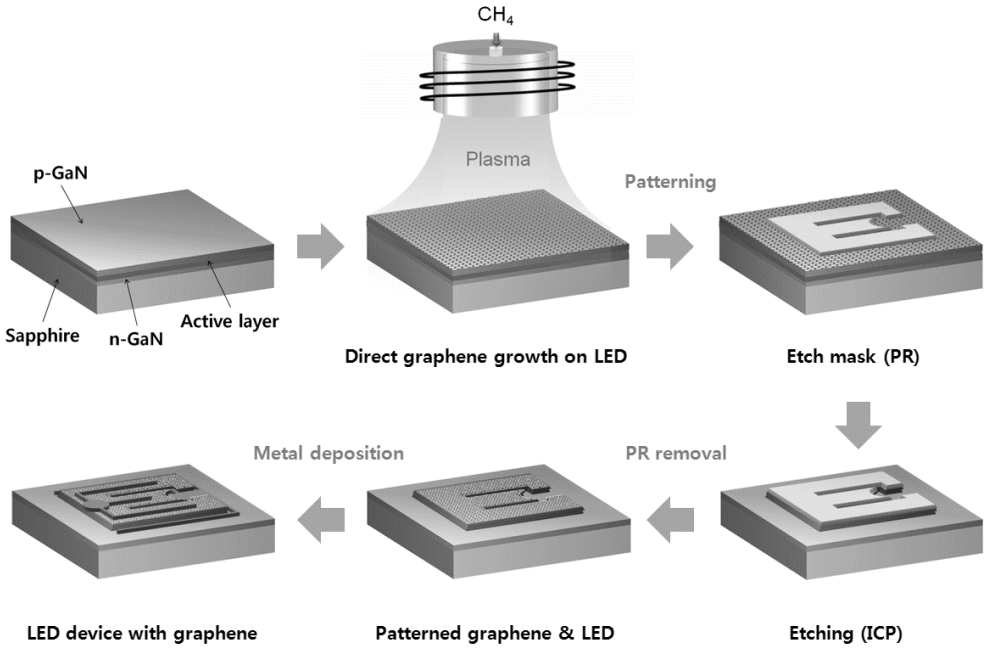

Figure 5. 17. Direct growth of polycrystalline graphene and fabrication process of DG/LED

Figure 5.18a shows an optical image of the DG/LEDs on 1x1 cm^2 wafer. To verify the functionality of DG on the p-GaN layer, the light output power (P_o) of the LEDs was investigated. An output power map of 35 DG/LEDs (marked as gray rectangles in Figure 5.18a) at 20 mA is presented in Figure 5.18c, showing good uniformity of P_o with mean and standard deviation values of 7.46 mW and 0.46 mW, respectively (Figure 5.18b).

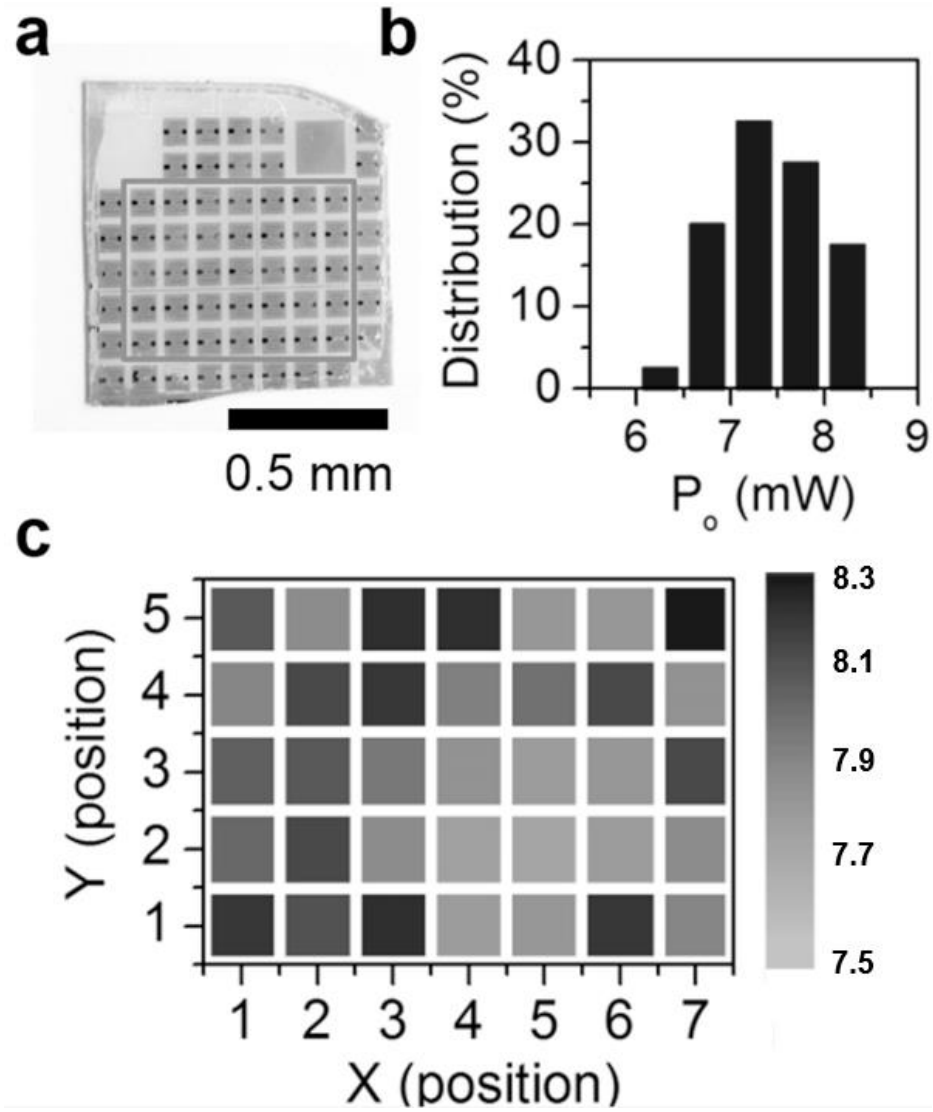

Figure 5. 18. (a) Optical images of the patterned devices on a 1 x 1 cm^2 substrate. (b) Distribution of the light output powers of 35 DG/LEDs (c) Light output power map over 35 DG/LEDs under the input current of 20 mA

Figure 5.19a compared the I–V characteristics of DG/LED and TG/LED. In case of TG/LED, the forward voltage is 4.8 V at 20 mA, which is analogous to the previously reported results for LEDs fabricated with transferred pristine graphene. As shown in the right-side inset of Figure 5.19a, the light emission of TG/LED is not uniform due to incomplete current spreading. In contrast, the forward voltage of the DG/LED is lowered to 4.1 V at 20 mA. Bright and uniform light emission patterns were observed for the DG/LED (left-side inset of Figure 5.19a), indicating that the DG electrode works well as a current spreading layer. Moreover, the DG/LED exhibited superior light output power (P_o) in comparison to the TG/LED as shown in Figure 5.19b.

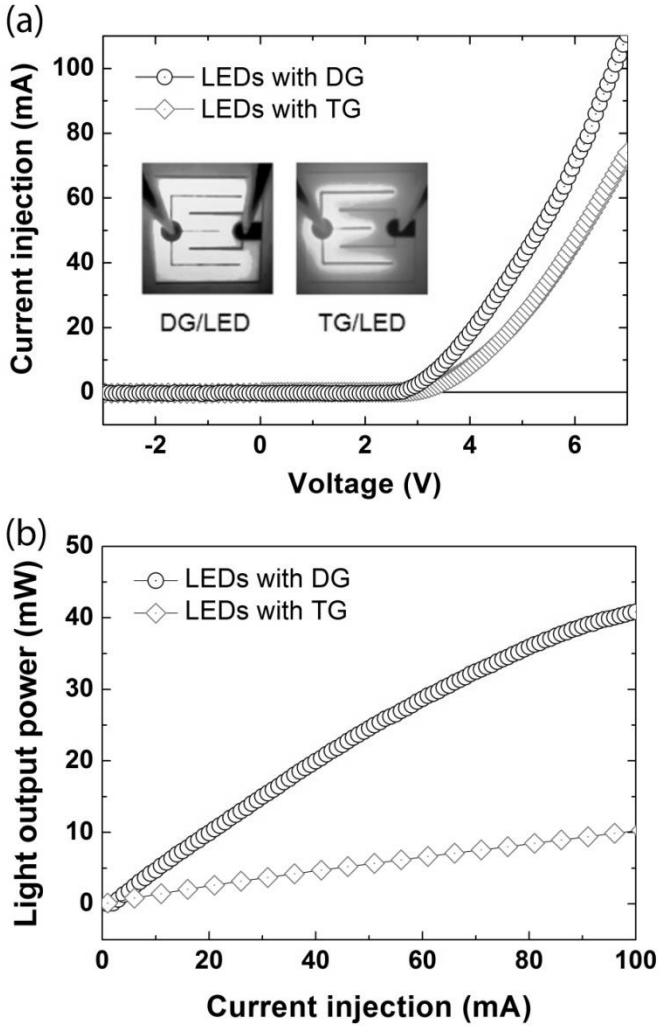

Figure 5. 19. (a) Current_voltage characteristics of LEDs with different electrodes. The insets show optical images of DG/LED (left) and TG/LED (right) after applying an input current of 20 mA. (b) Light output powers of DG/LED and TG/LED as a function of the input current

Considering the fact that the sheet resistance of DG (~1.0 kΩ/square, see Methods) is higher than that of TG (~0.6 kΩ/square), the enhanced electrical performance of DG/LED indicates that there are other important parameters for improved device performances and current spreading for LED. We found that plasma-assisted direct integration of graphene on LED resulted in carbon diffusion into p-GaN and *in situ* ohmic contact formation between graphene and p-GaN. Figure 5.20a shows secondary ion mass spectrometry (SIMS) profiles of C_{12} intensity for bare and graphene-grown p-GaN substrates, which suggest that carbons are diffused into p-GaN with a depth of 200–300 nm during plasma-assist graphene growth. The diffused carbon could act as a deep-level acceptor in the form of an interstitial atom or in the complex form with some defects.

To evaluate the DG/p-GaN contact, the current–voltage (I−V) characteristics and specific contact resistance (ρ_c) are measured by transmission line method. As shown at Figure 5.20b, a strong nonlinear behavior is observed in TG/p-GaN which can be attributed to many factors such as the adhesion and the Schottky barrier between the two layers, and evenness of graphene surface in contact with the GaN. On the contrary, linear I−V curve is observed in DG/p-GaN showing the ohmic behavior even at low

voltage range. Presumably the ohmic contact is established through the increased carrier concentration which is known to reduce the width of tunneling barrier, followed by the enhancement of carrier tunneling through the barrier. A specific contact resistance (ρ_c) of 0.15 Ω cm^2 is estimated from the gap spacing dependence of resistance (the inset of Figure 5.20b). The calculated ρ_c is comparable to the value of 0.6−5.5 Ω cm^2 reported for a graphene/p-GaN contact tailored with thin Ni/Au interlayer. These result indicate that ohmic contact formation and reduced contact resistance improved current spreading and performances of DG/LEDs.

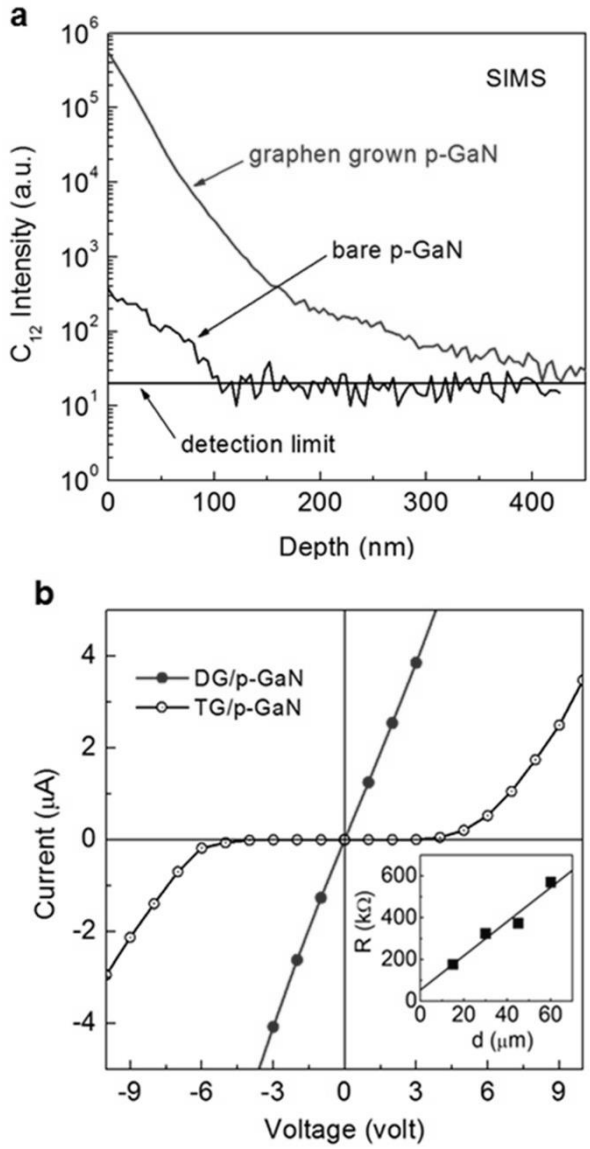

Figure 5. 20. (a) SIMS profiles of C12 intensity for virgin and graphene grown p-GaN. (b) I-V characteristics of DG/p-GaN and TG/p-GaN contacts. The inset shows gap spacing dependence of resistance for specific contact resistance calculation.

5.3. Reference

[1] K. S. Novoselov, A. K. Geim, S. V. Morozov, D. Jiang, Y. Zhang, S. V. Dubonos, I. V. Grigorieva and A. A. Firsov, *Science* **306**, 666-669 (**2004**).

[2] A. K. Geim and K. S. Novoselov, *Nat Mater* **6**, 183-191 (**2007**).

[3] Y. B. Zhang, Y. W. Tan, H. L. Stormer and P. Kim, *Nature* **438**, 201-204 (**2005**).

[4] K. S. Kim, Y. Zhao, H. Jang, S. Y. Lee, J. M. Kim, K. S. Kim, J. H. Ahn, P. Kim, J. Y. Choi and B. H. Hong, *Nature* **457**, 706-710 (**2009**).

[5] X. S. Li, W. W. Cai, L. Colombo and R. S. Ruoff, *Nano Lett* **9**, 4268-4272 (**2009**).

[6] J. W. Suk, A. Kitt, C. W. Magnuson, Y. F. Hao, S. Ahmed, J. H. An, A. K. Swan, B. B. Goldberg and R. S. Ruoff, *Acs Nano* **5**, 6916-6924 (**2011**).

[7] X. S. Li, Y. W. Zhu, W. W. Cai, M. Borysiak, B. Y. Han, D. Chen, R. D. Piner, L. Colombo and R. S. Ruoff, *Nano Lett* **9**, 4359-4363 (**2009**).

[8] H. Medina, Y. C. Lin, C. H. Jin, C. C. Lu, C. H. Yeh, K. P. Huang, K. Suenaga, J. Robertson and P. W. Chiu, *Adv Funct Mater* **22**, 2123-2128 (**2012**).

[9] H. Bi, S. R. Sun, F. Q. Huang, X. M. Xie and M. H. Jiang, *J Mater*

Chem **22**, 411-416 (**2012**).

[10] J. H. Hwang, V. B. Shields, C. I. Thomas, S. Shivaraman, D. Hao, M. Y. Kim, A. R. Woll, G. S. Tompa and M. G. Spencer, *J Cryst Growth* **312**, 3219-3224 (**2010**).

[11] K. B. Kim, C. M. Lee and J. Choi, *J Phys Chem C* **115**, 14488-14493 (**2011**).

[12] J. Sun, N. Lindvall, M. T. Cole, K. B. K. Teo and A. Yurgens, *Appl Phys Lett* **98**, 252107 (**2011**).

[13] H. Medina, Y.-C. Lin, C. Jin, C.-C. Lu, C.-H. Yeh, K.-P. Huang, K. Suenaga, J. Robertson and P.-W. Chiu, *Adv Funct Mater* **22**, 2123-2128 (**2012**).

[14] L. C. Zhang, Z. W. Shi, Y. Wang, R. Yang, D. X. Shi and G. Y. Zhang, *Nano Res* **4**, 315-321 (**2011**).

[15] A. C. Ferrari and J. Robertson, *Phys Rev B* **61**, 14095-14107 (**2000**).

[16] A. C. Ferrari, *Solid State Commun* **143**, 47-57 (**2007**).

[17] J. A. Mucha, D. L. Flamm and D. E. Ibbotson, *J Appl Phys* **65**, 3448-3452 (**1989**).

[18] Y. Muranaka, H. Yamashita, K. Sato and H. Miyadera, *J Appl Phys* **67**, 6247-6254 (**1990**).

[19] X. L. Li, G. Y. Zhang, X. D. Bai, X. M. Sun, X. R. Wang, E. Wang and H. J. Dai, *Nat Nanotechnol* **3**, 538-542 (**2008**).

Chapter 6

Conclusion

Single layer graphene films were grown on 25 μm thick Cu foils by PECVD. Uniform and large scale graphene were obtained and analyzed by utilizing AFM, SEM, TEM, TEM, and Raman spectroscopy. As the plasma power is increased, the grain size increases at low plasma power (10~50 W) and decreases at higher plasma power (>50W), showing a saturation behavior when the plasma power is higher than 120 W. The effect of substrate temperature on graphene growth is investigated while the plasma power and the growth time were maintained at 50 W and 3 minutes. As the temperature decreases, the ratio of I_D/I_G increases from 0.2 to 0.7 and I_{2D}/I_G decreases from 4.0 to 2.2. Even at the substrate temperature of 700 ℃, however, the ratio of I_{2D}/I_G is higher than 2 and a single-Lorentzian 2D peak is observed, indicating that a single layer graphene was synthesized with some defects. As a result, single layer graphene showed good transmittance of larger than 90% for wavelengths ranging from 200 to 800 and 600 ohm/sq.

Secondly, it was found that the quality of graphene after the device

fabrication was a critical factor affecting the performance of GaN-based LEDs. The qualities of graphene after two different device fabrication processes were evaluated by Raman spectroscopy and. It was found that graphene was severely damaged and split into submicrometer-scale islands bounded by less conducting boundaries when graphene was transferred onto LED structures prior to the GaN etching process for p-contact formation. On the other hand, when graphene was transferred after the GaN etch and p-contact metallization, graphene remained intact and the resulting InGaN/GaN LEDs showed electrical and optical properties that were very close to those of LEDs with 200 nm thick ITO films. The forward-voltages and light output powers of LEDs were 3.03 V and 9.36 mW at an injection current of 20 mA, respectively.

Thirdly, we show that direct graphene growth without a catalyst is possible on the InGaN/GaN LED substrate at temperatures as low as 500 ℃ using PECVD. The film consists mainly of few-layer polycrystalline graphene, confirmed by transmission electron microscopy and Raman spectra. With few-layer graphene directly grown on GaN- based epitaxial grown substrates, LEDs could be fabricated without transfer process and resulting LEDs showed uniform light output power distribution and superior performances over tens of devices. These indicated that direct graphene growth provides various

advantages of uniform interface and reliable performance in addition to transfer-free device fabrication, which could be adopted easily in the industrialization of graphene

Abstract in Korean

탄소 원자 한 층의 2차원 물질인 그래핀은 지금까지 알려진 물질 중에 가장 얇고, 전기나 열을 잘 전달 할 수 있을 뿐 아니라 높은 투과도 및 강한 인장력을 가지면서 유연한 물질로써 이를 활용한 다양한 연구가 활발하게 시도되고 있다. 특히, 광반도체 분야에서 그래핀이 종례에 투명전극으로 주로 사용되고 있는 인듐산화주석(indium tin oxide)를 대체할 수 있을 것이라을 대체하기 위한 실험을 위해 많은 연구 그룹들이 연구를 진행 중이다.

최초로 그래핀을 발광다이오드에 인듐산화주석을 대신하여 적용한 실험 결과가 2010년 발표되었으나, 기대에 훨씬 못 미치는 동작특성을 보여줌으로써 발광 다이오드에 그래핀 적용을 위한 많은 과제를 안겨주었다. 이러한 이유로는 성장된 그래핀을 전사하는 과정에서 발생하는 다양한 오염원 혹은 그로부터 발생되는 그래핀의 특성 저하가 원인된다. 따라서, 본 연구에서는 그래핀 전극을 채택한 발광 다이오드의 공정 과정을 개선하며 더 나아가 그래핀 전극 형성 과정에서 발생할 수 있는 그래핀 특성 악화 인자를 규명하고자 하였다. 또한, 기존의 전사 공정으로 도중 발생될 수 있는 금속 잔류물로부터의 그래핀 전극의 박막 특성 악화를 원천적으로 차단할 수 있는 새로운 기술인 그래핀 직접 성장법을 개발 하고자 하였으며 전사 방식과 직접 성장 방식으로 형성된 그래핀과 기판의 계면의 특성에 대한 연구를 진행하였다.

본 연구에서는 첫 번째로, 구리 촉매기판을 사용하여 CVD로 성장된 단일층 그래핀을 사용하였다. 또한, 비교군으로 제작된 인듐산화주석의 경우 전자빔증착방식으로 형성 후 RTA 처리를 하여 완성되었다. MOCVD를 이용하여 통상적인 방식으로 성장된 갈륨질소(GaN) 기반의 발광다이오드 기판을 토대로 인듐산화주석 전극을 채택한 발광다이오드와 그래핀 기반으로 제작된 발광다이오드를 제

작하였다. 발광다이오드의 제작 공정은 최근 그래핀 발광 다이오드 제작을 위하여 폭 넓게 사용되는 방식을 채택하였다. n형 전극은 두 가지 모두의 경우 동일하게 TiAlTiAu를 사용하였으며, 변수를 최소화 하기 위하여 그래핀 발광 다이오드의 경우 열처리 공정을 배제하고 실험을 진행하였다. 또한, 공정 초기와 후기에 그래핀 전극을 형성한 샘플을 각각 준비하여 발광 다이오드 제작 완료 후 그래핀 박막의 특성을 라만 분석 및 원자탐침현미경을 통하여 관측하였다. 그 결과 공정 초기에 그래핀 전극을 형성한 소자의 경우 그래핀의 격리(isolation) 현상이 발생하여 전극으로써의 역할을 수행하지 못하게 됨을 관측하였다. 이러한 현상의 원인은 식각공정 도중 사용하는 플라즈마 처리였는데 그래핀 상부에 보호막층으로써 3마이크로 미터의 포토레지스트를 코팅해 놓았지만 공정 도중 플라즈마가 그래핀의 막질에 영향을 미칠 수 있다는 것을 실험적으로 확인하였다. 결과적으로 그래핀 막질의 저하가 발생하지 않은 그래핀 기반 발광다이오드의 경우 막질저하가 일어난 그래핀 발광다이오드에 비해서 20mA 구동전류를 기준으로 3.9V에서 3.03V로 감소하였으며, 광출력은 7.72mW에서 9.36mW로 증가되었다.

두 번째로, 그래핀 박막을 금속 촉매 기판을 사용하지 않으면서 추가적인 공정이 필요 없는 그래핀 직성장 기술을 개발하고자 하였다. 그래핀 직성장 기술이란 니켈(Ni), 구리(Cu)와 백금(Pt) 등의 전위금속(transition metal)을 사용하지 않고 기판위에 직접 그래핀 박막을 성장 하는 기술을 말한다. 전위금속을 이용해 성장된 그래핀 박막은 필수불가결하게 추가적인 금속제거를 위한 식각공정을 거쳐야 하는데 이로 인한 오염 및 그래핀 막질의 특성저하가 발생하게 된다. 그래핀 직성장 기술의 장점은 첫째, 금속 촉매를 사용하여 성장된 그래핀을 식각하여 전사하여 사용하는 기존의 그래핀 전사 공정을 수반하지 않는다. 즉, 태생적으로 추가적인 금속식각 공정을 필요치 않는다. 추가적인 공정으로부터 야기되는 막질저하를 피할 수 있다. 두 번째, 비등방성(isotropic) 그래핀 박막 형성이 가능하다. 이는 그래핀 전극을 기존의 반도체 공정들과 유사한 방

식으로 형성하는 것을 가능케 하였다는 데 큰 의의가 있으며, 포토마스크 및 메탈마스크를 사용한 선택적 박막형성 공정을 가능하게 한다. 세 번째, 균일하고 깨끗한 계면특성을 보이는 박막 성장이 가능하며 박막 두께가 쉽게 조절 가능하다.

세 번째로, 다양한 그래핀 형성 방법에 따른 그래핀 박막과 기판의 계면 특성에 관한 연구를 진행하였다. 앞서 언급된 전사 방식과 직성장 방식을 통해 제작된 각각의 발광 다이오드의 계면에 대한 연구를 통해 각각의 그래핀 전극 형성 방법의 장점과 단점 그리고 계면에 대한 특성을 연구하였다.

주요어: 발광 다이오드, 그래핀 직접성장 기술, 그래핀 발광 다이오드

학 번: 2009-31186

List of publications

Journal papers

1. Yong Seung Kim*, **Kisu Joo**, Sahng-Kyoon Jerng, Jae Hong Lee, Euijoon Yoon and Seung-Hyun Chun "Direct growth of patterned graphene on SiO_2 substrates without the use of catalysts or lithography", ***Nanoscale,*** 6, 10100 (2014). (IF = 6.414)
2. Bumho Kim, Daeyoung Moon, **Kisu Joo**, Sewoung Oh, Youngkuk Lee, Yongjo Park, Yasushi Nanishi and Euijoon Yoon, "Investigation of leakage current paths in n-GaN by conductive atomic force microscopy", ***Appl. Phys. Lett.***, **104**, 102101 (2014). (IF = 3.794)
3. **Kisu Joo***, Yong Seung Kim*, Jae Hong Lee, Sahng-Kyoon Jerng, Euijoon Yoon, Seung-Hyun Chun, "Direct Integration of Polycrystalline Graphene into Light Emitting Diodes by Plasma-Assisted Metal-Catalyst-Free Synthesis", ***ACS nano,*** **8**, 3, 2230 (2014). (IF = 12.06)
4. Jonghak Kim*, Heeje Woo, **Kisu Joo**, Sungwon Tae, Jinsub Park, Daeyoung Moon, Sung Hyun Park, Junghwan Jang, Yigil Cho, Jucheol Park, Hwnakuk Yuh, Gun-Do Lee, In-Suk Choi, Yasushi Naishi, Heung Nam Han, Kookheon Char, and Euijoon Yoon, "Less strained and more

efficient GaN light-emitting diodes with embedded silica hollow nanospheres", ***Sientific Reports, 3***,*3201* (2013). (IF = 2.93)

5. Sahng-Kyoon Jerng*, **Kisu Joo**, Youngwook Kim, Sang-Moon Yoon, Jae Hong Lee, Miyoung Kim, Jun Sung Kim, Euijoon Yoon, Seung-Hyun Chun, and Yong Seung Kim* "Ordered growth of topological insulator on amorphous surface: a case study of Bi_2Se_3 thin films on dielectric SiO_2 substrates", ***Nanoscale, 5,*** *10618* (2013). (IF = 6.414)
6. Yong Seung Kim*, Jae Hong Lee, Young Duck Kim, Sahng-Kyoon Jerng, **Kisu Joo**, Eunho Kim, Jongwan Jung, Euijoon Yoon, Yun Daniel Park, Sunae Seo, Seung Hyun Chun, "Methane as an effective hydrogen source for single-layer graphene synthesis on Cu foil by plasma enhanced chemical vapor deposition", ***Nanoscale***, **5**, 1221 (2013). (IF = 6.414)
7. **Kisu Joo***, Sahng-Kyoon Jerng, Yong Seung Kim, Bumho Kim, Seunghyun Moon, Daeyoung Moon, Gun-Do Lee, Yoon-Kyu Song, Seung-Hyun Chun, and Euijoon Yoon, "Reduction of graphene damages during the fabrication of InGaN/GaN light emitting diodes with graphene electrodes", ***Nanotechnology***, **23**, 425302 (2012). (IF = 3.979)
8. Jae-Kyung Choi*, Jae-Hoon Huh, Sung-Dae Kim, Daeyoung Moon, Duhee Yoon, **Kisu Joo**, Jinsung Kwak, Jae Hwan Chu, Sung Youb Kim,

Kibog Park, Young-Woon Kim, Euijoon Yoon, Hyeonsik Cheong and Soon-Yong Kwon, "One-step graphene coating of heteroepitaxial GaN films", ***Nanotechnology,* 23**, 435603 (2012). (IF = 3.979)

9. S. H. Park*, J. Park, D.-J. You, **K. Joo**, D. Moon, J. Jang, D.-U. Kim, H. Chang, S. Moon, Y.-K. Song, G.-D. Lee, H. Jeon, J. Xu, Y. Nanishi, and E. Yoon, "Improved emission efficiency of a-plane GaN light emitting diodes with silica nano-spheres integrated into a-plane GaN buffer layer", ***Appl. Phys. Lett.***, 100, 19 (2012). (IF = 3.844)